Energy Conversion and Management 341 (2025) 120055

Contents lists available at ScienceDirect

Energy Conversion and Management

journal homepage: www.elsevier.com/locate/enconman

Research Paper

# Multiparameter optimization of torrefaction for achieving carbon-negative biocoal: integrating quality parameters, thermodynamics, and environmental performance

Giulia Cruz Lamas [a], Thiago da Silva Gonzales [a], Simone Monteiro [a], Pedro Paulo de Oliveira Rodrigues [a], Lucélia A. Macedo [b], Thiago O. Rodrigues [c], Patrick Rousset [d], Thiago de Paula Protásio [e], Armando Caldeira Pires [a], Edgar A. Silveira [a,*]

[a] University of Brasília, Mechanical Sciences Graduate Program, Laboratory of Energy and Environment, Brasília, DF, Brazil
[b] Forest Products Laboratory, Brazilian Forest Service, Brasília 70818900, Brazil
[c] Brazilian Institute of Information in Science and Technology, Brasília, DF, Brazil
[d] CIRAD, UPR BioWooEB, F-34398 Montpellier, France
[e] Federal University of Lavras – UFLA, Department of Forest Science, 37203-202 Lavras, Minas Gerais, Brazil

ARTICLE INFO

*Keywords:*
Carbon Sequestration
Energy Efficiency
Global Warming Potential
Thermochemical Conversion
Sustainable Biofuel Production
Circular Economy

ABSTRACT

This study advances the torrefaction field by proposing a framework that integrates energy, exergy, and environmental analyses with the quality assessment of torrefaction products, while evaluating process carbon neutrality and carbon-negative outcomes. While biocoal properties are often emphasized, multi-objective analyses addressing critical aspects such as exergy efficiency and life cycle assessment are frequently overlooked. This research critically addresses inconsistencies in life cycle assessment related to functional units, system boundaries, and impact allocation of products, fostering a consistent and robust environmental diagnostic. Experimental data from urban forest waste torrefaction, combined with a two-step kinetic modeling, enabled the simulation of a scaled-up system using Aspen Plus. This integrative approach assessed the properties of biocoal, bio-oil, and torgas, as well as mass and energy flows, irreversibilities, and process emissions. Life cycle assessment quantified and allocated environmental impacts. The framework accounted for $CO_2$ uptake by biomass, revealing trade-offs arising from the severity of torrefaction and the definition of the functional unit. Response surface methodology served as a unifying optimization tool, allowing the simultaneous integration and evaluation of all indicators. Results identified bottlenecks, formulated an equation to evaluate carbon neutrality and determined optimal conditions, offering a scalable and replicable pathway for sustainable torrefaction. Optimal conditions at 256 °C for 41 min yielded biocoal with 87.82 % mass retention, a heating value of 20.98 MJ $kg^{-1}$, a fuel ratio of 0.34, and an ash content of 4.98 %. The system required 20.99 kWh for drying and 4.04 kWh for torrefaction, with the irreversibility of 81.5 MJ $h^{-1}$ and a global warming potential of –0.504 kg $CO_2$ eq. per GJ of biocoal.

## 1. Introduction

Lignocellulosic residues from agricultural and forest management represent an abundant and renewable feedstock for sustainable bioenergy production [1]. Their use contributes to greenhouse gas mitigation and supports the transition to low-carbon energy systems [2]. In Brazil, the availability of biomass resources has stimulated efforts to replace fossil-based energy with renewable alternatives [3]. However, raw biomass presents critical limitations, such as high moisture content, low energy density, and heterogeneous composition [4], requiring pretreatment to improve its suitability as a fuel [5].

Torrefaction is a mild thermochemical pretreatment carried out in inert or low-oxygen environments, typically between 200 and 300 °C [6]. This process upgrades raw biomass into a hydrophobic, energy-dense, and stable solid fuel commonly referred to as biocoal [7]. By promoting the partial degradation of hemicelluloses and cellulose, torrefaction improves grindability, combustion behavior, and fuel properties [8]. Despite these advantages, the process, along with its auxiliary subsystems and logistics, consumes energy and generates emissions [9],

* Corresponding author.
*E-mail address:* edgar.silveira@unb.br (E.A. Silveira).

https://doi.org/10.1016/j.enconman.2025.120055
Received 17 March 2025; Received in revised form 4 June 2025; Accepted 7 June 2025
Available online 25 June 2025

**Nomenclature**

| | |
|---|---|
| AP | Acidification Potential |
| ANOVA | Analysis of Variance |
| ASH | Ashes |
| $CO_2$ | Carbon Dioxide |
| CO | Carbon Monoxide |
| C | Carbon |
| RSM | Response Surface Methodology |
| SCB | Specific Chemical Bioexergy |
| TETP | Terrestrial Ecotoxicity Potential |
| UFW | Urban Forestry Waste |
| VM | Volatile Matter |
| EP | Eutrophication Potential |
| FC | Fixed Carbon |
| FAETP | Freshwater Aquatic Ecotoxicity Potential |
| FU | Functional Unit |
| GWP | Global Warming Potential |
| GHG | Greenhouse Gas |
| HHV | Higher Heating Value |
| HTP | Human Toxicity Potential |
| H | Hydrogen |
| LCA | Life Cycle Assessment |
| LCI | Life Cycle Inventory |
| MAETP | Marine Aquatic Ecotoxicity Potential |
| $N_2$ | Nitrogen gas |
| N | Nitrogen |
| O | Oxygen |
| ODP | Ozone Layer Depletion Potential |
| POCP | Photochemical Ozone Creation Potential |

*Symbols*

| | |
|---|---|
| $C_{\%,raw}$ | Carbon content |
| $i$ | Chemical compound |
| $Q_{dryer}$ | Drying energy consumption |
| $E$ | Emission factor |
| $h$ | Enthalpy |
| $s$ | Entropy |
| $x$ | Molar fraction |
| $MM$ | Molar Mass |
| $I$ | Irreversibility |
| $A$, $B$, $C$, $V_1$, $V_2$ | Pseudocomponents |
| $\varepsilon$ | Random error |
| $\beta_i$ | Regression coefficients |
| $A$ | RSM input temperature |
| $B$ | RSM input time |
| $ex^0_{ch}$ | Standard chemical exergy value |
| $T$ | Temperature |
| $t$ | Time |
| $Q_{tor}$ | Torrefaction energy consumption |
| $Y_{TS}$ | Solid yield |
| $VM_{TS}$ | Volatile yield |

highlighting the need for a comprehensive sustainability evaluation [10].

Standard experimental investigations of torrefaction often involve thermogravimetric analysis [11] or small-scale furnaces [12], providing insight into mass loss and thermal decomposition [11]. Nevertheless, these setups offer limited information on energy requirements and scalability. Simulation tools, such as Aspen Plus®, have been employed to model mass and energy balances of torrefaction reactors, thereby enhancing the understanding of process behavior under varying operational conditions [12]. Simulating biomass conversion under varying conditions enables the prediction of process outcomes and energy consumption. It offers insights into the feasibility of large-scale applications,

**Table 1**
Literature summary on torrefaction modeling on Aspen Plus.

| Feedstock | Type (Exp./ Modeling) | Products / Analysis | Assessment | Optimization / Criteria | Ref. |
|---|---|---|---|---|---|
| Corn residue pellets | **Exp.:** Torrefaction<br>Temp.: 220–300 °C<br>Time: 20 min<br>**Num.:** Aspen Plus | **Biocoal:** Yield, Ultimate, and Calorific<br>**Volatiles:** Yield | **1E**<br>Energetic | None | [15] |
| Pinewood chips | **Exp.:** Torrefaction<br>Temp.: 230–290 °C<br>Time: 30 min<br>**Num.:** Aspen Plus | **Biocoal:** Yield, Ultimate, and Calorific<br>**Volatiles:** Yield | **1E**<br>Energetic | None | [16] |
| Spent coffee grounds and coffee husk | **Exp.:** Torrefaction<br>Temp.: 200–300 °C<br>Time: 30–60 min<br>**Num.:** Aspen Plus | **Biocoal:** Ultimate, Proximate, and Calorific | **2E**<br>Energetic<br>Environmental | None | [12] |
| *Eucalyptus globulus* and *Pinus radiata* | **Exp.:** Torrefaction<br>Temp.: 250 and 280 °C<br>Time: 15 and 30 min<br>**Num.:** Aspen One | **Biocoal:** Yield, Ultimate, Proximate, and Calorific<br>**Volatiles:** Yield and Calorific | **2E**<br>Energetic<br>Exergy | None | [17] |
| Norwegian birch branches | **Exp.:** Torrefaction<br>Temp.: 240–300 °C<br>Time: 30 min<br>**Num.:** Aspen Plus | **Biocoal:** Yield, Ultimate, and Calorific<br>**Volatiles:** Yield | **1E**<br>Energetic | Curve intersection / Biocoal quality<br>Process energy efficiency | [18] |
| Rice husk | **Exp.:** Torrefaction<br>Temp.: 220–340 °C<br>Time: 30–90 min<br>**Num.:** Aspen Plus | **Biocoal:** Yield, Ultimate, and Calorific | **1E**<br>Energetic | RSM / Biocoal quality | [19] |
| Urban forest waste | **Exp.:** Torrefaction<br>Temp.: 225–275 °C<br>Time: 20–60 min<br>**Num.:** Aspen Plus | **Biocoal:** Yield, Ultimate, Proximate, and Calorific<br>**Bio-oil:** Yield, Ultimate, and Calorific<br>**Volatiles:** Yield, Ultimate, and Calorific | **3E**<br>Energetic<br>Environmental (LCA)<br>Exergy | RSM / Biocoal quality<br>Process exergy efficiency<br>Life cycle assessment | This study |

identifies potential efficiency bottlenecks, and generates data inventories for further evaluations [13], supporting system optimization. Recent studies have employed Response Surface Methodology (RSM) to optimize torrefaction parameters, specifically temperature and residence time [14]. These approaches primarily focus on improving fuel quality metrics, such as heating value and solid yield (Table 1). However, comprehensive optimization that integrates product quality, process irreversibility and environmental impacts remains scarce.

In this context, Life Cycle Assessment (LCA) is recognized for quantifying the potential environmental burdens within energy systems [2]. In torrefaction studies, methodological inconsistencies in LCA, particularly in functional units, allocation methods, and carbon uptake accounting, hinder accurate assessment (Table 2). Moreover, the environmental contribution of bio-oil and torgas is frequently overlooked, and cradle-to-grave analyses are scarce. These discrepancies complicate process evaluation and its potential for scaling up.

This research integrates process upscale modeling and LCA within a multi-objective optimization framework to evaluate torrefaction performance from both technical and environmental perspectives. Experimental data and validated kinetic modeling of a torrefaction plant in Aspen Plus enabled the simulation of wood waste under specified conditions to assess torrefaction outcomes. Thermodynamic efficiency is analyzed through exergy calculations, with process irreversibility explicitly included as a performance indicator. These thermodynamic insights, interpreted as system energy and mass flows, are coupled with an LCA to quantify environmental impacts throughout the process. The LCA adopts a cradle-to-grave perspective, allocating environmental burdens among biocoal, bio-oil, and torgas and examining the influence of functional unit selection (mass-based vs. energy-based) across a broad set of impact categories. All performance indicators (fuel quality, exergy efficiency, and environmental impacts) are integrated into a multi-objective optimization using RSM. By also considering the yields and fuel properties of bio-oil and torgas, this approach offers a complete view of energy-environmental trade-offs. The result is a robust and scalable method to optimize torrefaction toward sustainable technology.

## 2. Material and methods

The following subsections detail the feedstock, modeling procedures, and environmental assessment methods used in this study.

### 2.1. Material

Urban forest waste (UFW), derived from routine pruning, is available year-round [25]. In Brasília, an efficient management system handles over 200 $m^3$ of green waste and 100 $m^3$ of logs daily, reflecting the city's five million urban trees [26]. The feedstock analyzed in this study was based on prior work by Silveira et al. [27], who characterized a blend of six hardwoods (*Ficus benjamina, Mangifera indica, Persea americana, Pelthophorum dubium, Tapirira guianensis, and Anadenanthera colubrina*) sourced from Brasília's urban forestry (Fig. 1(a)). The blend presented 31.00 % moisture, 77.61 % db. volatile matter, 17.90 % db. fixed carbon, and 4.49 % db. ash. On a dry basis (db), it contained 44.91 % db. carbon, 7.25 % db. hydrogen, 0.64 % db. nitrogen, and 42.71 % db. oxygen, making it suitable for torrefaction upgrade. Detailed information in the supplementary material (SM) describes the characterization procedures and the properties of individual species and the UFW blend (Table S1), revealing low compositional variability among the six hardwoods.

### 2.2. Numerical modeling of torrefaction

The numerical modeling of the torrefaction process integrates kinetic and property prediction models within Aspen Plus®. Kinetic model and reaction rates data from Silveira et al. [27] support the simulation of solid yield dynamics, while empirical correlations and literature data inform property estimations. The torrefaction plant model, previously developed and validated by Gonzalez et al. [28], was applied to simulate the specific conditions evaluated in this study, allowing for the quantification of energy requirements and emissions.

Mass and energy balances from this simulation feed the LCA, while RSM was applied to optimize process parameters for improved biocoal quality, reduced irreversibilities, and minimized environmental impacts. All mathematical formulations and configurations required for the modeling are detailed in the SM and previous works.

#### 2.2.1. Estimation of solid and volatile yield and properties

This study employs the two-step reaction model by Di Blasi and Lanzetta [29], originally developed for hemicelluloses, to simulate the torrefaction of urban forestry waste (UFW). Previously applied to UFW in past research [27] and validated for other lignocellulosic biomasses [12], the model is fully described and formulated in Eqs. (S1–S8) of the

**Table 2**
Literature summary on recent LCA research of torrefaction process applied to lignocellulosic biomass.

| Biomass / Region | Contributions | Conversion technologies / System boundaries | Functional unit | Software Methodology | Allocation | $CO_2$ Uptake | Ref/ Year |
|---|---|---|---|---|---|---|---|
| Rice husk / California, USA | Decentralized torrefaction at rice mills as a cost-effective and eco-friendly option | Cradle-to-gate / Harvesting, drying, milling, torrefaction (240 and 300 °C, for 30 min), grinding, and densification | 1 MJ torrefied biomass | OpenLCA TRACI 2.1 | Mass / Energy / Economic | Not discussed | [20] 2020 |
| Microalgal / Taiwan, China | Conventional and oxidative torrefaction assessed to determine optimal conditions for energy efficiency and environmental impact | Gate-to-gate / Torrefaction (200, 250, and 300 °C; for 15, 30, 45, and 60 min) | 10 g raw biomass | OpenLCA CML2001 | None | Not discussed | [21] 2022 |
| Corncob / Harbin City, China | Mild torrefaction improves fuel properties with a low environmental impact | Gate-to-gate / Torrefaction (200, 225, 250, 275, and 300 °C; for 15, 30, 45, and 60 min) | 5 g raw biomass | OpenLCA CML2001 | None | Not discussed | [22] 2022 |
| Rice straw / Taiwan, China | Torrefaction effects on properties, microstructure, and environmental impact of biofuel | Gate-to-gate / Torrefaction (200, 225, 250, 275, and 300 °C; for 60 min) | 10 g raw biomass | OpenLCA ReCiPe and CML2001 | None | Not discussed | [23] 2022 |
| Torrefied spent coffee grounds / Taiwan, China | Torrefaction methods compared for biomass upgrading by cost and environmental impact | Gate-to-gate / Torrefaction (200, 250, and 300 °C; for 15, 30, 45, and 60 min | 8 g raw biomass | OpenLCA CML2001 | None | Not discussed | [24] 2023 |
| Urban forest waste / Brasília, Brazil | Optimized torrefaction for scalable biofuel with high biocoal quality, energy efficiency, and potential for carbon neutrality | Cradle-to-grave / Drying, torrefaction (225, 250, and 275 °C; for 20, 30, and 60 min), combustion | 1 GJ torrefied biomass | SPhera (GaBi) CML2001 | Mass / Energy | Yes | This study |

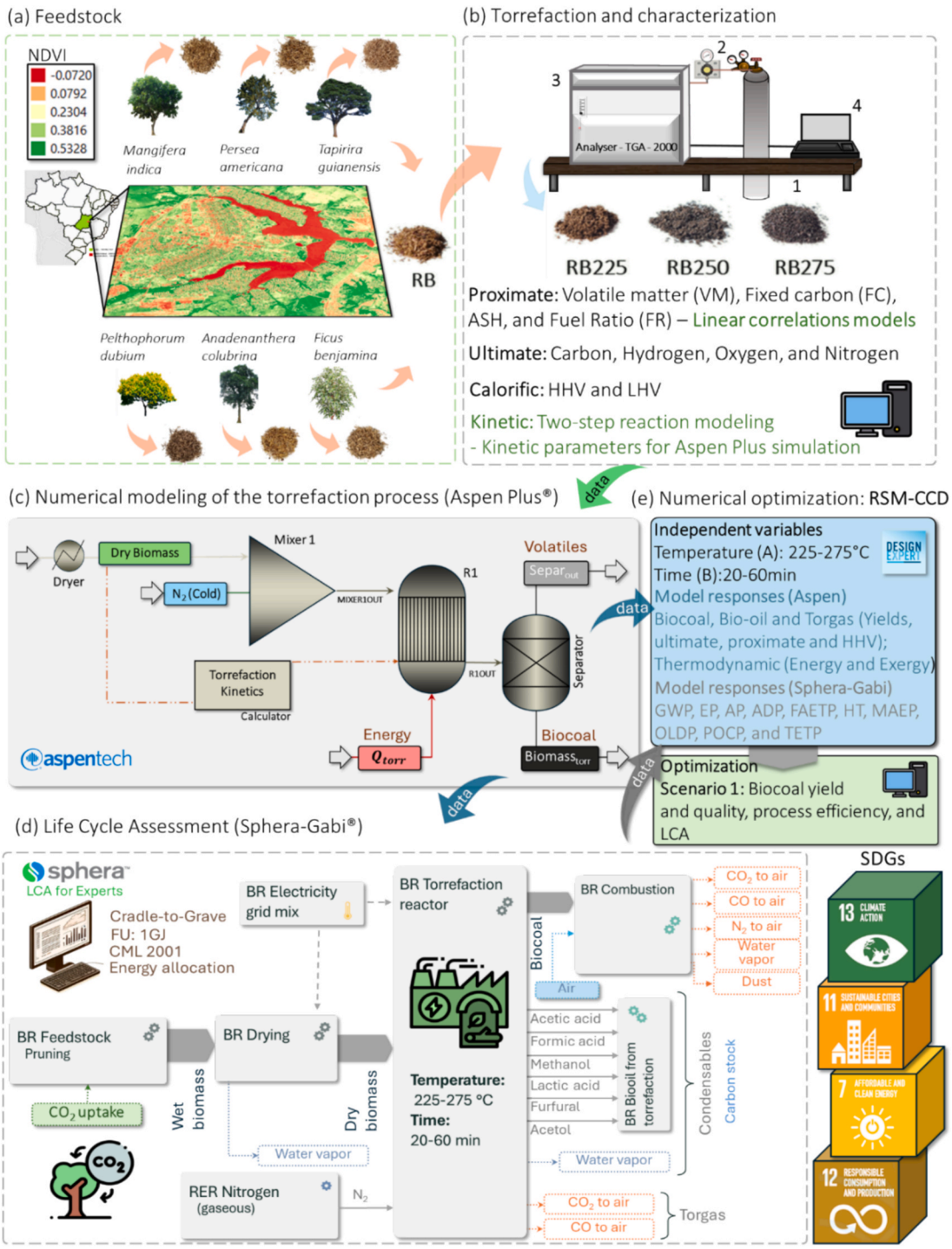


**Fig. 1.** (a) Description of the selected feedstock for the investigation [27]. (b) Torrefaction apparatus, experimental analysis and kinetic modeling to characterize the raw and torrefied blend [27] (detailed in SM). (c) Modeling of the torrefaction process in Aspen Plus. (d) LCA illustration highlighting system boundaries, input and output flows. (e) Description of optimization highlighting model responses obtained through the integrated approach.

SM. Kinetic parameters, also from [27], demonstrated strong agreement with experimental TGA data ($R^2 > 0.98$; see Table S2 and Fig. S1) and were adopted in the present modeling. The model and its associated kinetics were integrated into Aspen Plus® to simulate the torrefaction process across the experimental conditions defined by the design of experiments in Section 2.5, enabling the prediction of solid and volatile yields as a function of temperature and residence time.

To integrate the estimation of biocoal proximate properties into Aspen Plus, this study employed empirical models previously obtained through experimental assessment of the UFW blend torrefaction [27]. These models are based on linear correlations between solid yield ($Y_{TS}$) and the proximate properties of the torrefied product. Specifically, the fixed carbon (FC) and volatile matter (VM) contents were calculated using Eqs. (1) and (2), while ash content (ASH) and the Fuel Ratio (FR) were defined by Eqs. (3) and (4) [36].

$$FC = -56.633 \times Y_{TS} + 73.724 \quad (1)$$

$$VM = 61.629 \times Y_{TS} + 16.905 \quad (2)$$

$$ASH = 100 - FC - VM \quad (3)$$

$$FR = FC/VM \quad (4)$$

Both raw and torrefied biomass were modeled as solid compounds consisting of C, H, O, N, and ash. The elemental composition of biocoal under varying torrefaction severities was estimated using kinetic modeling combined with CHNO-based volatile release, as described in [30]. In the absence of experimentally determined volatile compositions for UFW, data from Prins [31] and Bates et al. [30] (see Table S3), originally derived from willow torrefaction, were adopted since this approach is commonly used in similar simulation studies [32].

The biocoal's HHV (MJ $kg^{-1}$), enhancement factor (EF, dimensionless), energy yield (EY, in %), and energy-mass coefficient index (EMCI, dimensionless) were determined by Eqs. (5)–(8).

$$HHV_{biomass} = 0.3491 \times C + 1.1783 \times H - 0.1034 \times O - 0.0151 \times N \quad (5)$$

$$EF = \frac{HHV_{biocoal}}{HHV_{raw}} \quad (6)$$

$$EY = Y_{TS} \times EF \quad (7)$$

$$EMCI = EY - Y_{TS} \quad (8)$$

#### 2.2.2. Torrefaction process modeling

This study applied a previously developed torrefaction model in Aspen Plus® V12.1 by Gonzales et al. [33]. The model, previously validated with experimental data from UFW torrefaction (225–275 °C, 20–60 min, 7 °C $min^{-1}$, inert atmosphere, dry biomass), as shown in Table S4 [28], was applied to simulate mass, energy, and exergy balances under the specific conditions of this study.

The plant (Fig. 1(c)) includes a simplified drying step, modeled with a HEATER block at 120 °C, which ensures the dry basis required for proximate analysis and prevents water recondensation. The stream $Q_{dryer}$ (in kJ $h^{-1}$) represents the energy required for drying. The process flowsheet uses three key output streams: "$Biomass_{torr}$" ($Y_{TS}$, biocoal %), "$Separ_{out}$" (volatiles %), and "$Q_{torr}$" (heat demand for torrefaction in kJ $h^{-1}$) (see Fig. 1(c)). A kinetic-based RYield reactor, combined with a calculator block, enables the dynamic simulation of product yields as functions of temperature and time. The descriptions of streams and blocks in Aspen Plus modeling are provided in Table S5 of the SM. Thermophysical properties were estimated using HCOALGEN and DCOALIGT models under isothermal and steady-state assumptions. Full process formulation, specifications and stream properties are detailed in previous literature [33] and the SM.

### 2.3. Exergy analysis

Exergy analysis was applied to assess the thermodynamic efficiency and irreversibilities ($I$) of the torrefaction process. The total exergy considered includes physical [34], chemical [35], and thermal contributions [36]. Physical exergy was calculated based on enthalpy and entropy differences relative to a reference environment (25 °C, 1 atm), while chemical exergy was estimated using standard values for volatile compounds (Table S6) and biomass composition (Table S4). The specific chemical bioexergy (SCB) of biomass was derived from its HHV. Thermal exergy was calculated from the heat demand at each torrefaction temperature. Process irreversibility, defined as the difference between total exergy inputs and outputs, was quantified to indicate entropy generation and resource losses [37]. This indicator was also integrated into the response surface methodology (RSM) as a response variable to identify optimal operating conditions that minimize exergy destruction. Formulations and details are provided in the literature [33] and the SM (Eqs. (S9–S15)).

### 2.4. Life cycle assessment

This section presents the LCA conducted to assess the potential environmental impacts of UFW torrefaction. The Goal and Scope of the LCA are covered by Sections 2.4.1–2.4.4, while Section 2.4.5 details the Life Cycle Inventory (LCI) of mass and energy flows. The analysis supports the process optimization framework by linking environmental performance to operating conditions.

#### 2.4.1. Functional unit

In LCA, the functional unit (FU) is a quantified description of the system's primary function used to normalize all inputs and outputs. Torrefaction involves a trade-off between improving energy quality and reducing biocoal yield. Higher torrefaction severities increase energy content in biocoal but require a greater amount of raw biomass to produce the same energy output. Therefore, the choice of the FU, whether "1 GJ of biocoal", "1 ton of raw biomass input", or "1 ton of biocoal output", can significantly influence the environmental assessment, as both solid yield and energy content vary with torrefaction severity. This study considers biocoal as a biofuel. Therefore, adopt a functional unit of 1 GJ of biocoal (torrefied biomass). To enable comparison with previous studies and to evaluate the influence of FU choice on LCA results, functional units of 1 ton of biomass input and 1 ton of biocoal output were also assessed.

#### 2.4.2. System boundaries and scenarios modeling

The system boundaries of the LCA encompass the cradle-to-grave bioenergy production chain, as illustrated in Fig. 1(d). Urban forestry operations are primarily performed for public safety, aesthetic purposes, and vegetation management rather than as a biomass supply chain. For this reason, residues are modeled as unavoidable co-products without allocation of upstream burdens. This approach aligns with standard LCA practices for waste streams where the upstream processes are unrelated to the intended valorization function [38]. Nevertheless, it incorporates the natural uptake of $CO_2$ promoted by the trees from the environment during their growth. Therefore, the system begins with the availability of pruned biomass and includes its drying, torrefaction, and the combustion of the produced biocoal. The LCA scenarios were established based on the conditions of the torrefaction process, as defined by the RSM (Section 2.5).

#### 2.4.3. Software, method and impact categories

Sphera's LCA for Experts software (v.10.9.0.20, formerly GaBi) with the Ecoinvent database (v.3.11) was employed, and the CML 2001 methodology was utilized according to the ISO 14040 series, following previous literature [24]. The CML 2001 method was applied to evaluate the associated carbon emissions, with special attention to the Global Warming Potential (GWP 100 years, kg $CO_2$ eq.). In addition to GWP, the study also presents, discusses, and compares ten other impact categories, including ADP elements: Abiotic Depletion (elements) (kg Sb eq.); ADP fossil: Abiotic Depletion (fossil) (MJ); Acidification Potential (AP, kg $SO_2$ eq.), Eutrophication Potential (EP, kg Phosphate eq.), Freshwater Aquatic Ecotoxicity Potential (FAETP, kg DCB eq.), Human Toxicity Potential (HTP, kg DCB eq.), Marine Aquatic Ecotoxicity Potential (MAETP, kg DCB eq.), Ozone Layer Depletion Potential (ODP steady state, kg R11 eq.), Photochemical Ozone Creation Potential (POCP, kg Ethene eq.), and Terrestrial Ecotoxicity Potential (TETP, kg DCB eq.). A comprehensive set of impact categories was selected based on prior research (Table 2), allowing for a direct comparison with multiple studies and an analysis of allocation in the environmental results.

#### 2.4.4. Environmental impacts and allocation

Few studies allocate environmental impacts among biocoal, bio-oil, and torgas (Table 2) since biocoal typically accounts for over 70 % of the yield. However, because torrefaction generates three energy-containing streams and given the increasing interest in bio-oil

valorization [39] and torgas re-circulation [40], impact allocation based on mass and energy criteria was applied for each stream.

#### 2.4.5. Life cycle inventory

The life cycle inventory (LCI) encompassed the input and outputs of materials, energy, and emissions to air, water, and soil [41]. The LCI is summarized in Table S7 for the FU of 1 GJ. Additionally, the LCI is presented in the FU of 1 ton of biocoal (Table S8), allowing for comparison with the literature. The carbon uptake ($CO_2$ *uptake*) was calculated as Eq. (9) [42].

$$CO_2\ uptake = Biomass_{db} \times C_{\%,raw} \times (MM_{CO_2}/MM_C) \quad (9)$$

Where $Biomass_{db}$ is the quantity of dry-basis raw biomass (kg) required to obtain 1GJ of biocoal or 1 ton of biocoal (for each specific torrefaction condition), $C_{\%,raw}$ stands for the carbon content on raw biomass (dry-basis) (Table 3), $MM_{CO_2}$ the molar mass of $CO_2$ equal to 44.01 g $mol^{-1}$ and $MM_C$ the molar mass of carbon (12.01 g $mol^{-1}$). The FU is critical in this calculation, which is directly influenced by torrefaction severity. As severity increases, biocoal yield decreases, requiring a higher amount of biomass to achieve the same energy content in biocoal. Consequently, the associated natural $CO_2$ uptake by biomass increases, as it is a function of the raw biomass input (Eq. (9)).

Potential environmental impacts depend on energy demand, nitrogen input, and emissions from torrefaction ($CO_2$ and CO). Aspen Plus simulations provided mass balances of raw biomass, biocoal, and volatiles (condensable and non-condensable gases, including $CO_2$, CO, and $H_2O$), as well as nitrogen and energy consumption ($Q_{dryer}$ and $Q_{torr}$). The emissions resulting from the combustion of the produced biocoal were evaluated using emission factors (kg $ton^{-1}$) for carbon monoxide ($E_{CO}$), carbon dioxide ($E_{CO_2}$), methane ($E_{CH_4}$), nitrogen oxides ($E_{NOx}$, primarily linked to the fuel-NOx mechanism, attributed to the oxidation of nitrogen present in the fuel), which are dependent on the emission factor of elemental carbon ($E_C$) [43]. In addition, the dust emission factor ($E_{dust}$, kg $ton^{-1}$) was estimated [44]. The calculations were based on Eqs. (S16–S21) in the SM, which employs the ultimate analysis of biomass along with an emission factor approach [45].

For each torrefaction condition (see Section 2.5), the $CO_2$ emissions generated during biomass conversion (torrefaction) and combustion were offset by the natural $CO_2$ uptake (Eq. (9)), maintaining a balanced carbon cycle. This equilibrium is a function of the degree of decarbonization, which depends on the amount of $CO_2$ captured by the feedstock (linked to the carbon content of the raw biomass) and the fraction of carbon retained in the resulting bio-oil (stored and not burned). In contrast, carbon emissions from drying (associated with energy consumption), torrefaction (due to torgas release and process energy demand), and combustion (related to the oxidation of biocoal carbon content) contribute to the net $CO_2$ output.

### 2.5. Torrefaction design and optimization

The severity of torrefaction significantly influences biocoal yield and quality (FR, ash and HHV), process efficiency (irreversibility), and, consequently, the environmental impacts [40]. Those properties were optimized by maximizing biocoal yield, FR, and HHV and minimizing ash content, irreversibility, and environmental impacts. The GWP was set to be lower than zero throughout optimization, conferring a "carbon–neutral" torrefaction. A design based on central composite design (CCD) with $\alpha = 1$ was employed, a common approach for optimization, including torrefaction [46]. Treatment temperature and time were considered "in range" for optimization.

Previous research has applied RSM to optimize biomass torrefaction, focusing on temperatures ranging from 200–300 °C and treatment times of 20–60 min [47]. In this study, a temperature range of 225–275 °C, a treatment time of 20–60 min, and a constant heating rate of 7 °C $min^{-1}$ were chosen to ensure the reproducibility of experimental data from [27]. The output data from the simulation on Aspen Plus and LCA for Experts were entered into Stat-Ease Design-Expert (version 23.1.4) for evaluation. Tables S9–S10 in SM further detail the build information for the RSM assessment of 30 30 model's responses ($R$) (Table S11) and the design used for numerical modeling.

The data obtained from numerical simulations were used to develop quadratic (Eq. (10)), reduced quadratic (Eq. (11)), and reduced cubic models (Eq. (12)) through stepwise regression. The highest non-aliased polynomial degree was selected for each case, retaining only statistically significant terms to minimize overfitting and multicollinearity [48].

$$R = \beta_0 + \beta_1 T + \beta_2 t + \beta_{12} Tt + \beta_{11} T^2 + \beta_{22} t^2 + \varepsilon \quad (10)$$

$$R = \beta_0 + \beta_1 T + \beta_2 t + \beta_{12} Tt + \beta_{11} T^2 + \varepsilon \quad (11)$$

$$R = \beta_0 + \beta_1 T + \beta_2 t + \beta_{12} Tt + \beta_{11} T^2 + \beta_{22} t^2 + \beta_{112} T^2 t + \beta_{122} Tt^2 + \varepsilon \quad (12)$$

Here, $\beta_i$ are the regression coefficients, $T$ (in °C) and $t$ (in min) are input temperature and time, and $\varepsilon$ is the random error. ANOVA, with a 95 % confidence level, assessed the model's accuracy. 3D surfaces were analyzed to visualize input variables' impact, interactions, and sensitivity on the torrefaction outcomes. The optimization of the torrefaction process was assessed using desirability-based criteria (detailed in Eqs. (S21–S23) in the SM).

## 3. Results and discussion

This section presents and discusses the simulation results from Aspen Plus, LCA, and RSM analyses. A comprehensive dataset supports the findings, with the complete data provided in the SM, to assist in interpreting the upcoming 3D surface plots, figures, and related discussions. The resulting model equations for the 30 analyzed responses are pre-

**Table 3**
Results for the separate system stages (feedstock, drying, torrefaction, and combustion) considering the average values for each LCA impact category across all evaluated torrefaction conditions (Run 1–Run 13), based on a functional unit of 1 GJ of biocoal.

| Categories | Electricity | | Torrefaction | | Combustion | Total |
|---|---|---|---|---|---|---|
| | Dryer | Torrefaction | Emissions | $N_2$ | Emissions | |
| **ADP elements** | 83.3 % | 16.7 % | – | 0.1 % | – | 100 % |
| **ADP fossil** | 83.3 % | 16.7 % | – | 0.1 % | – | 100 % |
| **AP** | 27.4 % | 5.5 % | – | – | 67.1 % | 100 % |
| **EP** | 15.5 % | 3.1 % | – | – | 81.4 % | 100 % |
| **FAETP** | 83.3 % | 16.7 % | – | – | – | 100 % |
| **GWP** [a] | 5.5 % | 1.1 % | 0.7 % | – | 92.7 % | 100 % |
| **HTP** | 70.3 % | 14.1 % | – | – | 15.6 % | 100 % |
| **MAETP** | 83.3 % | 16.7 % | – | – | – | 100 % |
| **ODP** | 83.2 % | 16.7 % | – | 0.1 % | – | 100 % |
| **POCP** | 1.2 % | 0.2 % | 2.7 % | 26.6 % | 69.3 % | 100 % |
| **TETP** | 83.3 % | 16.7 % | – | – | – | 100 % |

[a] Feedstock carbon capture was not included in this analysis.

sented in Table S11, considering only the statistically significant variables identified in the ANOVA results (Table S12). All quadratic and reduced models (quadratic and cubic) showed strong statistical significance ($p < 0.05$). The models demonstrated high regression accuracy with $R^2$ values exceeding 0.92 (Table S13). The equations in Table S11 are expressed in terms of actual factors – temperature ($T$, in °C) and time ($t$, in min) – allowing torrefaction outcomes and environmental impact prediction within 225–275 °C and 20–60 min, using the assessed feedstock. The corresponding results for each response, considering biocoal quality, process efficiency and environmental impacts, are further illustrated and discussed. In addition, for easy access to data and results transparency, Tables S14–S16 provide the simulation results (yields and properties) of biocoal, bio-oil, torgas, and thermodynamic properties.

### 3.1. Torrefaction yields

Fig. 2(a) presents the design of simulations, addressing each simulation run to the specific torrefaction condition. While Fig. 2(b) presents a ternary diagram constrained to three aggregated product categories – biocoal, bio-oil (including water), and torgas – Fig. 2(c) provides a more detailed resolution of the volatile stream, considering the relative composition of the volatile fraction only. In this figure, water is represented as a distinct component, rather than being grouped within the bio-oil fraction, to emphasize its significant quantitative contribution to the total volatile yield.

As the severity of torrefaction increased, a significant variation in product distribution was revealed, as expected. Lower temperatures and shorter durations favor biocoal production, with a minimal volatile release, while higher temperatures lead to increased bio-oil and torgas production, decreasing the biocoal yield (Tables S14–S16). Fig. 2 shows the decrease of biocoal yield from 97.73 % to 75.3 % (Fig. 2(d)), bio-oil production increased from 0.69 % to 18.39 % (Fig. 2(e)), water released ranging between 1.05–4.64 % (Fig. 2(f)) and torgas ranged from 0.53 % to 1.84 % (Fig. 2(g)), aligning with the torrefaction products standard range [2]. Consistent biocoal retention across runs suggests torrefaction can be tuned to optimize yield, quality, and volatile production, depending on targets like maximizing bio-oil or recovering heat via gas re-circulation.

The increase in torrefaction severity reflects the trade-off between biocoal yield, its energy density enhancement, and related volatile production (which can be further employed for burning and re-circulation or as bio-oil). During light torrefaction (Runs 1, 6, and 13), water release is closely linked to dehydration mechanisms of cellulose and hemicelluloses breakdown, the least thermally stable biomass component [49]. At 225 °C, the high water content indicates that moisture is removed without significant decomposition of complex organic compounds. For example, water release drops from 46 % in Run 1 to 43 % in Run 13 (225 °C, 60 min). This shows that light torrefaction primarily removes moisture, while hemicelluloses decompose via deacetylation, releasing mainly acetic acid and water [50]. Evaluating the water and bio-oil % (Fig. 2(c)), a shift from moisture-driven volatiles at low temperatures to complex organic breakdown as temperatures rise. In Run 1, water dominates the volatiles (46.2 %), while bio-oil is minimal (30.3 %). At 275 °C (Run 9), bio-oil reaches 44.4 % of the volatiles, overtaking water (18.77 %).

Acetic acid and water were the main liquid products at low torrefaction severity, with methanol, lactic acid, and hydroxyacetone becoming more prevalent at higher temperatures, aligned to [51]. Cellulose decomposition yields levoglucosan and other anhydrosugars, though levoglucosan is unstable and further breaks down into volatiles such as water, methanol, acetic acid, acetone, and phenols [52]. The increasing presence of formic acid, acetic acid, and hydroxyacetone correlates with hemicelluloses decomposition, followed by cellulose and lignin at higher temperatures (275 °C) [32]. Acid-catalyzed hemicelluloses hydrolysis produces pentose (C5) and hexose (C6) sugars, with subsequent pentose dehydration forming furfural [52].

The decarboxylation of carboxyl groups (–COOH) in the hemicelluloses structure results in the release of $CO_2$ as a significant component of the torrefaction gas stream [49]. Hemicelluloses decomposition primarily releases $CO_2$ and CO as its polymer structure breaks down [51]. This decomposition accounts for most of the gas release during the initial stages of the process. As the hemicelluloses decompose, the percentage of CO and $CO_2$ in the volatile gases decreases (Fig. 2 (c)), even as the total volume of torgas slightly increases (Fig. 2(g)). The non-volatile content remains relatively stable throughout the runs, with the $CO_2$/CO ratio diminishing over time. This aligns with theoretical expectations since CO is generated in secondary reactions, consistent with the simulation conditions [51]. The $CO_2$/CO decreases from 4.85 to 4.57 as the temperature increases from 225 to 275 °C, consistent with the literature, which reports a decline from 6.5 to 2.5 within the 200–300 °C range [53].

### 3.2. Quality of torrefaction products

Fig. 3 illustrates the stoichiometric CHO diagram for the torrefaction products, highlighting the changes in elemental composition as torrefaction severity increases. Additionally, the Van Krevelen diagram of biocoal is presented, allowing for comparison with literature data, and the 3D response surfaces for the calculated HHVs of biocoal, bio-oil, and torgas are displayed. Tables S14–S16 display the yields (in %) and properties of biocoal, bio-oil, and torgas. The carbon content in biocoal increases gradually from 45.52 % at 225 °C for 20 min to 49.41 % at 275 °C for 60 min, while the oxygen content decreases from 41.98 to 36.91 %, indicating a carbonization process.

The biocoal H/C and O/C ratios decline with increasing temperature and time, with the H/C dropping from 1.90 to 1.66 and the O/C from 0.69 to 0.56 (Fig. 3(e) and Table S14). These reflect the removal of hydroxyl and methoxyl groups as hemicelluloses decompose and lignin depolymerizes [50]. The biocoal transformation leads to a more stable and energy-dense biofuel, as evidenced by the increase in HHV from 20.08 to 21.51 MJ $kg^{-1}$ (Fig. 3(f)). Fig. 3(b) and (e) support the coalification process, showing the decrease in H/C and O/C ratios in the biocoal compared to raw biomass and other biocoals, such as *Pinus elliottii* [54] and *Eucalyptus* sp. [55]. Bio-oil retains a higher oxygen content, starting at 54.49 % at 225 °C for 20 min and decreasing to 52.32 % at 275°C for 60 min (Table S15), derived from the biocoal deoxygenation process. Table S15 shows that the H/C of bio-oil (2.28 to 2.58) remains higher than biocoal throughout the process, indicating a greater degree of carbonization and aromatic structure formation in the biocoal.

The HHV of bio-oil starts at 14.91 MJ $kg^{-1}$ and increases to 17.05 MJ $kg^{-1}$ with rising temperature and time (Fig. 3(g)). This trend demonstrates torrefaction's positive impact on both bio-oil and biocoal, with biocoal benefiting from lower oxygen content, higher carbon content, and FC. Torgas shows a relatively low HHV, starting at 1.74 MJ $kg^{-1}$ at 225 °C and increasing slightly to 1.83 MJ $kg^{-1}$ at 275 °C (Fig. 3(h)). Its composition remains consistent, with a carbon content of 30 % and an oxygen content of ~ 70 % (Table S16), indicating that the gas is primarily a low-energy by-product compared to bio-oil and biocoal. Fig. 4 presents the evaluation of the proximate properties of biocoal, along with the assessment of HHV, EY, and EMCI of biocoal.

As seen in Fig. 4(a), the proximate properties of biocoal shift significantly towards the top corner with increasing torrefaction severity. Overall, the observed ranges in Table S14 of FC (18.38 % to 31.10 %), VM (63.29 % to 77.14 %), and ash (4.49 % to 5.61 %) are consistent with the reaction governing the decomposition of

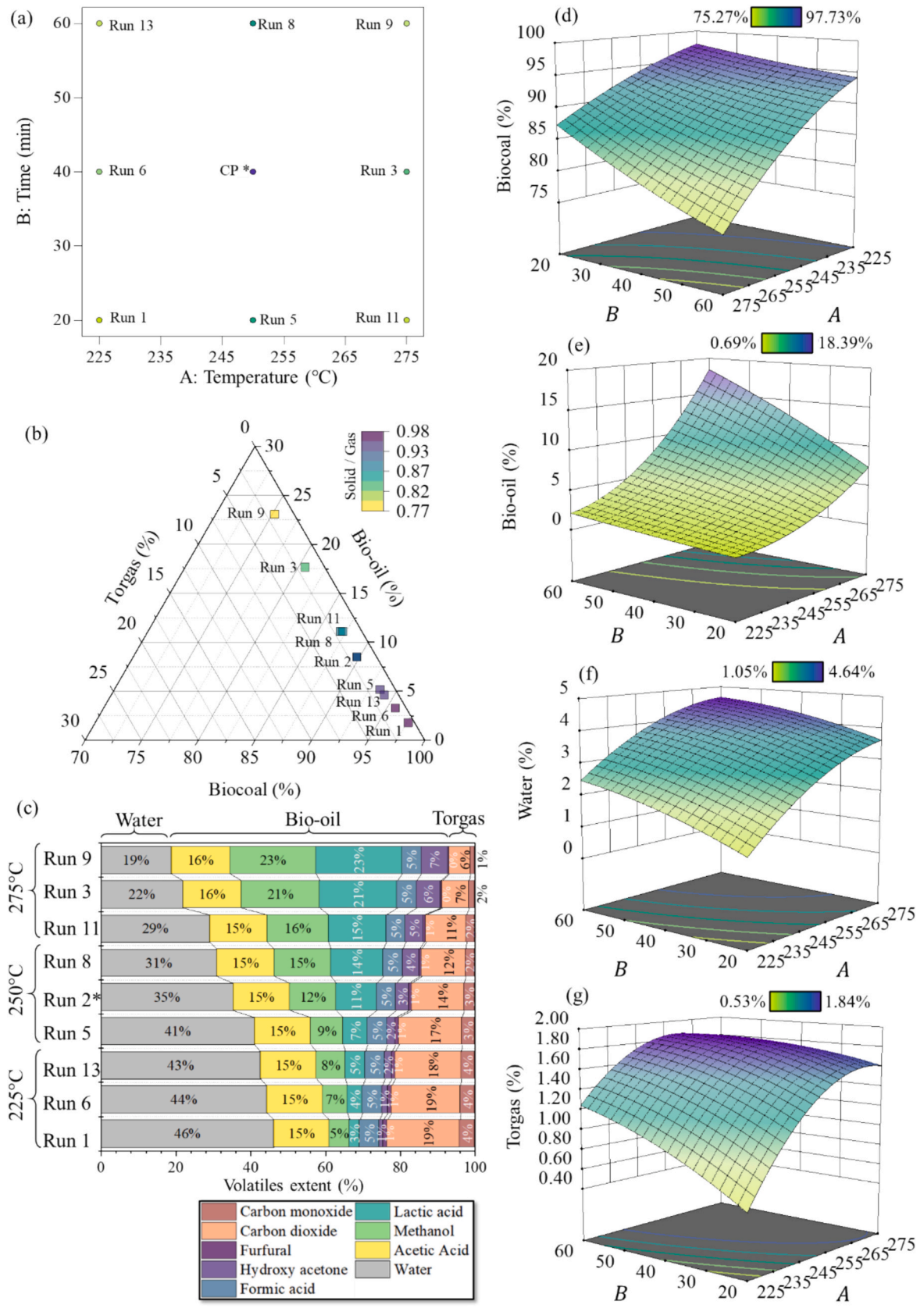


**Fig. 2.** (a) The design of simulations specifying the torrefaction temperatures (*A* in °C) and times (*B* in min). CP stands for central point contemplating five points, which includes runs 2, 4, 7, 10, and 12. (b) Ternary diagram for the mass balance of torrefaction products (biocoal, bio-oil including water fraction, and torgas). (c) Stacked columns show the relative composition of the volatile fraction only. 3D surfaces for (d) biocoal, (e) bio-oil, (f) water, and (g) torgas.

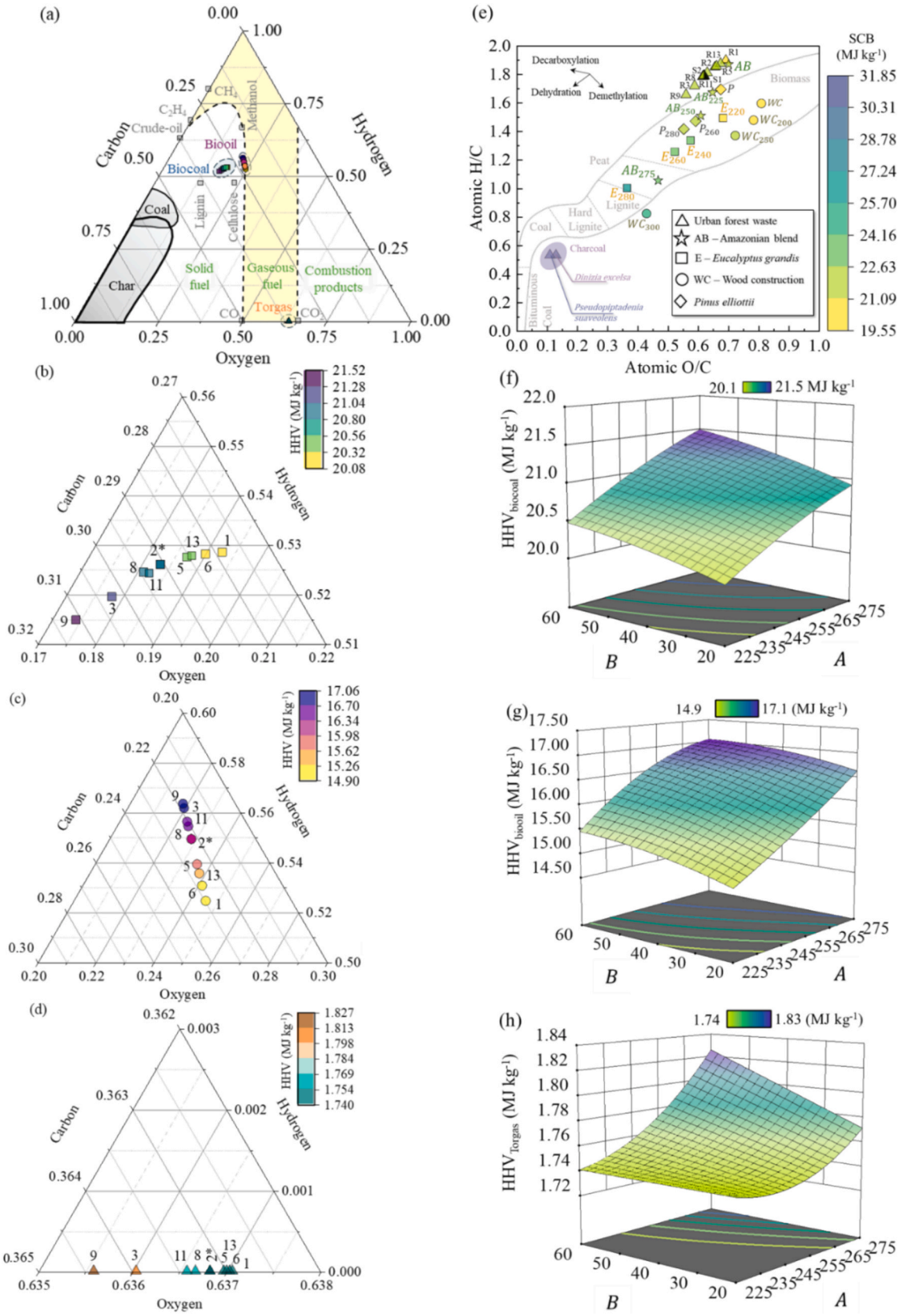


**Fig. 3.** (a) Stoichiometry diagram (CHO) for (a) all torrefaction outcomes, (b) biocoal, (c) bio-oil and (d) torgas. (e) Van Krevelen diagram of biocoal with literature comparison: Amazonia Charcoal [56]; *Pinus elliottii* (P–raw and 300 °C [54]), *Eucalyptus* sp. (E–raw, 240–280 °C [55]), Amazon blend (AB – raw, 225–275 °C) [57] and wood construction waste (WC – raw, 225–275 °C [9]. 3D surface for HHV of biocoal (f), bio-oil (g), and (h) torgas (in MJ $kg^{-1}$), respectively, for torrefaction temperatures (*A* in °C) and times (*B* in min).

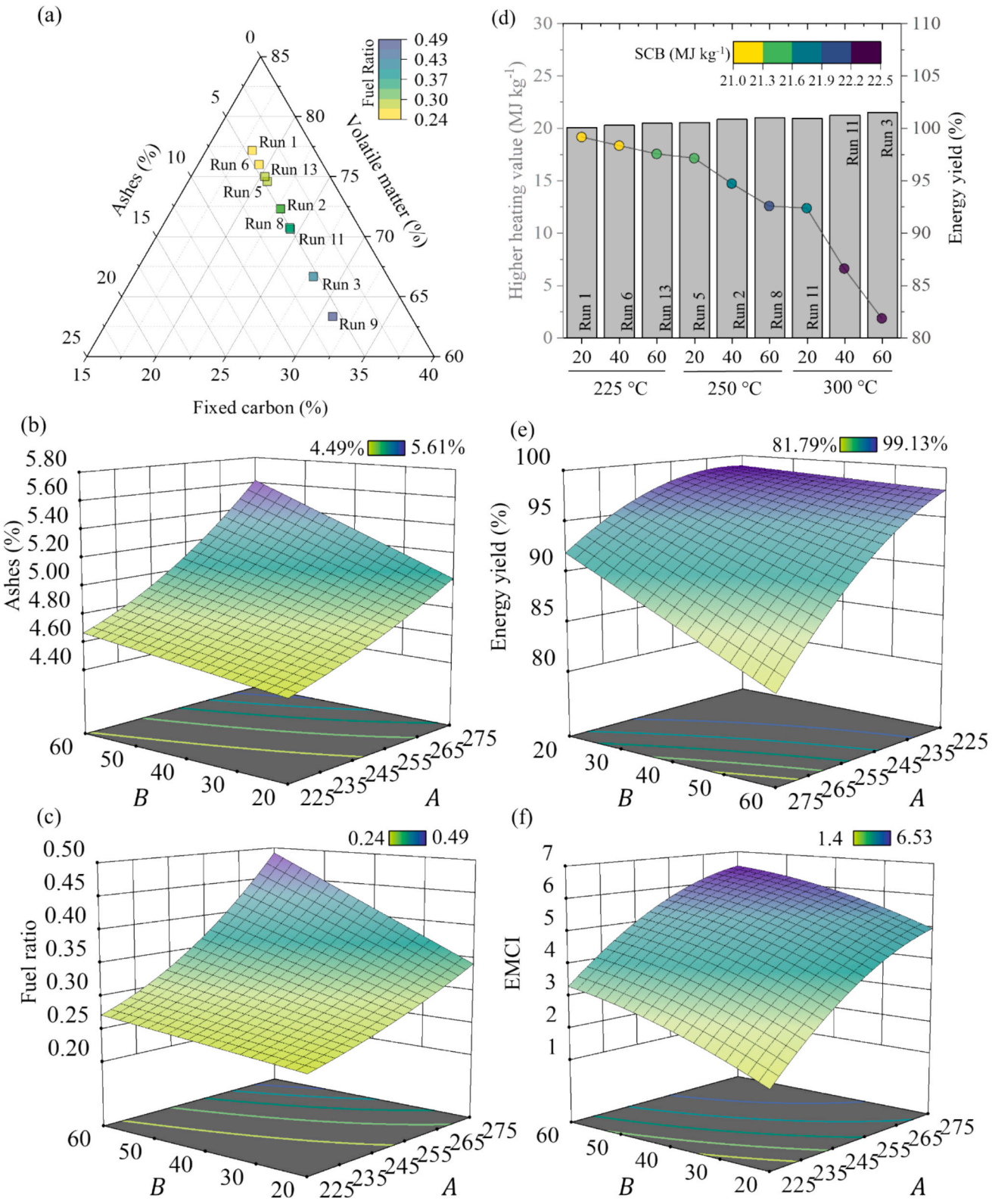


**Fig. 4.** (a) Ternary diagram for the proximate properties of biocoal. (b) Response surface for Ashes (in %) and (c) Fuel ratio (FR) considering the model's independent parameters: *A* (temperature in °C) and *B* (time in min). (d) Stack columns for higher heating value (HHV), energy yield (EY) (points), and specific chemical bioexergy SCB (colormap) of biocoal. Response surface of (e) EY and (f) Energy-mass coefficient index for torrefaction temperature (*A* in °C) and times (*B* in min).

hemicelluloses, cellulose, and lignin during torrefaction.

The HHV and EY are displayed in Fig. 4(d). While the HHV increases, the EY decreases from 99.13 % to 81.80 % (Fig. 4(e)) over the same range due to the reduction of biocoal yield, resulting in a variation between 1.4 and 6.53 of EMCI (Fig. 4(f)). These trade-offs highlight the importance of carefully regulating process conditions to optimize biocoal quality while maintaining energy efficiency.

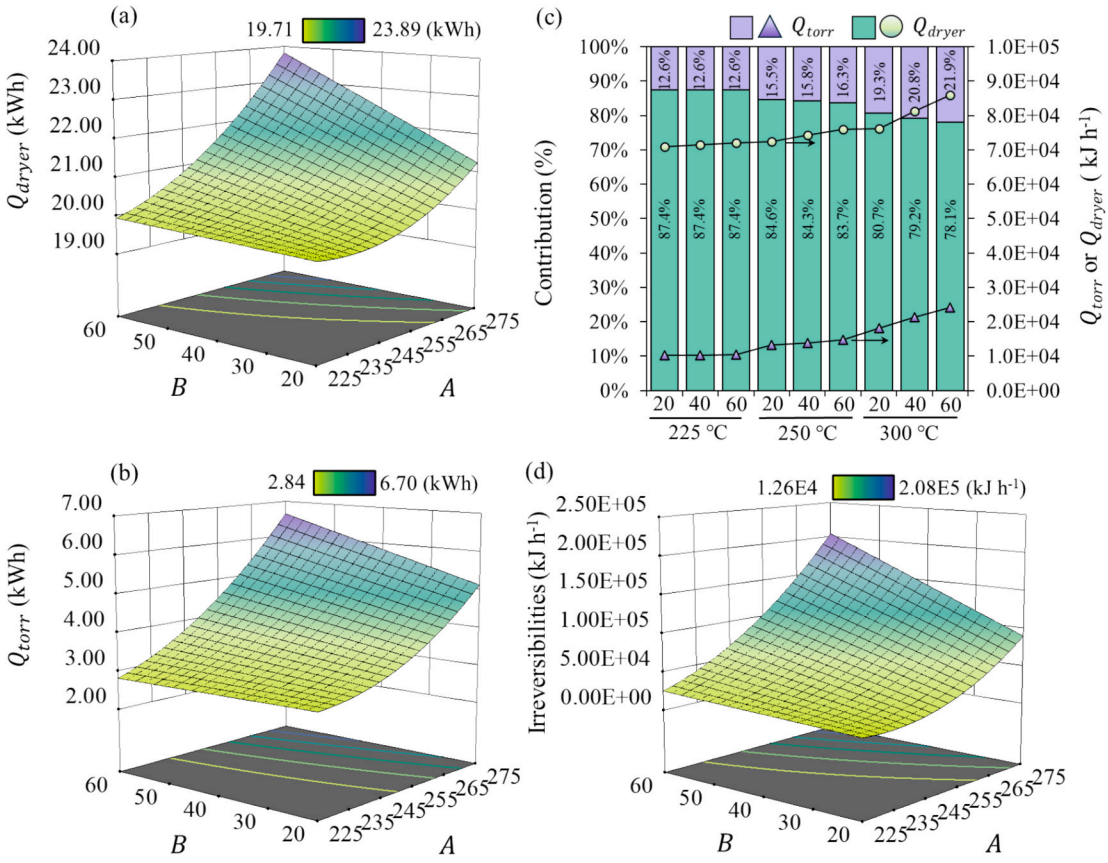


**Fig. 5.** Response surface for (a) $Q_{dryer}$ (in kWh), (b) $Q_{torr}$ (in kWh), and (d) Irreversibilities (in kJ h$^{-1}$), considering the model's independent parameters: *A* (temperature in ∘C) and *B* (time in min) and the FU of 1 GJ. (c) stack columns for the contribution in % of $Q_{torr}$ and $Q_{dryer}$ and markers for the $Q_{torr}$ and $Q_{dryer}$ values in kJ h$^{-1}$.

### 3.3. Energy requirement analysis

Fig. 5 shows the energy requirement of drying and torrefaction ($Q_{dryer}$ and $Q_{torr}$, in kWh) processes, along with the torrefaction irreversibilities (in kJ h$^{-1}$) as a function of process temperature and time considering the functional unit (FU) set to 1 GJ of biocoal. Table S17 also provides $Q_{torr}$ in MJ h$^{-1}$ and kJ kg$^{-1}$ of UFW for literature comparison.

The energy demand for the drying process ($Q_{dryer}$) was 1392.37 kJ per kilogram of dried biomass, equivalent to approximately 0.4 kWh kg$^{-1}$. This value aligns with the literature, which reported around 0.5 kWh kg$^{-1}$ under similar process conditions in Aspen Plus [58]. Since the heat quantity for the drying process depends on the amount of biomass (kJ per kilogram of dried biomass), it is essential to emphasize the choice of the FU in LCA, which will influence this calculation. If the FU is set to 1 ton of input biomass, the heat required for drying will remain constant without accounting for variations related to the torrefaction process. Conversely, if the FU is based on 1 ton of torrefied biomass, it would consider the biocoal yield reduction; however, it would overlook the inherent trade-offs between biocoal yield and HHV. Aligning the FU with the energy purpose of the product (FU of 1 GJ) allowed for the recalculation of the heat required for drying (see Fig. 5(a)) as a function of the torrefaction temperature and time, better reflecting the variation in biocoal's SY and HHV. The recalculated $Q_{dryer}$ ranged between 19.71 and 23.89 kWh (70.95–85.99 MJ kg$^{-1}$), increasing with torrefaction severity conditions since a higher biomass input flow (consequently more heat for drying) is required for severe torrefactions.

Considering torrefaction conditions of 225–275 °C and 20–60 min, $Q_{torr}$ ranged from 2.84 to 6.70 kWh in Fig. 5(b) (corresponding to 200 to 391 kJ kg$^{-1}$ for torrefying a 1 kg h$^{-1}$ of dried biomass). These values are consistent with the literature, where experimental studies and predictive models have recorded torrefaction heat values ranging from –387 to 540 kJ kg$^{-1}$, considering different biomasses (beech, spruce and willow) and torrefaction conditions (220–300 °C, 10–60 min) [2].

Fig. 5(a), (b), and (c) indicate that the thermal energy required increases as the severity of the treatment rises due to the higher energy demand needed to reach higher temperatures and longer residence times. Moreover, it reveals that drying is the most energy-intensive stage [59]. Manouchehrinejad and Mani [60] and Bach et al. [18] note that drying accounts for approximately 80 % of total energy requirements, depending on the process conditions, which aligns with the results (78–87 %) in Fig. 5(c).

Fig. 5(d) and Table S17 show that irreversibility ranged between (12.56–207.53 MJ h$^{-1}$) and increases with rising energy demand as the torrefaction process becomes more severe, an expected result once the exergy destruction of a heat flow is related to temperature. Another factor contributing to the increase in irreversibility is the reduction in biocoal yield (see Fig. 2(d)). Although energy quality improves, the decrease in biocoal yield as torrefaction severity increases is directly linked to the rise in exergy destruction (a small portion of this exergy is transferred to the volatiles, while irreversibilities destroy the remainder). The conclusions from this section are specific to the yield and composition of the UFW used, as well as the selected torrefaction parameters. Differences in reactor design, feedstock properties, heating rates, or atmospheres may alter conversion dynamics and energy performance.

### 3.4. Life cycle assessment

The RSM analysis resulted in quadratic, reduced quadratic, and cubic models for the assessed environmental categories (see model equations

in Table S11). Table 3 presents the results for the separate system stages (feedstock, drying, torrefaction, and combustion), showing the averaged values for each LCA impact category across all evaluated torrefaction conditions (Runs 1–13) for a functional unit (FU) of 1 GJ of biocoal. This enabled a detailed discussion and identification of the contributions of each stage to the process. In addition, Fig. S2 in the SM shows the 3D surfaces as a function for torrefaction temperature and time, obtained from these models, based on an FU of 1 GJ of biocoal. The results cover a temperature range of 225–275 °C and reaction times from 20 to 60 min. The tabulated results of Fig. S2, along with the results for FU of 1 ton of output biocoal, are also presented in Table S18 for further discussion, as mass-based FU is the standard in the torrefaction literature.

Fig. S2 illustrates the potential environmental impacts, showing likely trends with fluctuations in intensity across the torrefaction conditions. Despite these variations, a consistent positive correlation emerges between temperature and treatment time, indicating that higher temperatures and extended treatment durations generally amplify the observed impacts. This can be attributed to the energy input requirement, higher temperatures and longer torrefaction durations lead to greater energy consumption and enhanced environmental impacts [23].

Table 6 shows that the stage of biocoal combustion was the largest source of emissions in the categories AP (67.1 %), EP (81.4 %), GWP (92.07 %), and POCP (69.3 %). In the categories where combustion does not contribute (ADP, FAETP, MAETP, ODP, TETP), electricity consistently emerges as the dominant process, accounting for an average of 99.96 %, primarily from the dryer (83.30 %), aligned to the $Q_{dryer}/Q_{torr}$ ratio (see Section 3.3). Meanwhile, emissions from the torrefaction (specifically CO and $CO_2$, referred to as torgas) are present in the GWP (0.7 %) and POCP (2.7 %) categories. The carrier gas ($N_2$) contributed minimally to ADP and ODP (around 1 %) and averaged 26.6 % to POCP. Table S19 also presents the values for the impact categories from which the contribution percentages in Table 6 were derived.

Comparing LCA results is challenging due to significant variations across studies. As shown in Table 2, each study uses distinct FU and system boundaries, leading to different conclusions. Notably, none address the impact of $CO_2$ uptake from biomass on GWP. In the present discussion, the FU was defined as producing 1 GJ of torrefied biomass (biocoal). However, to compare the results of this study with the literature, a harmonization protocol was conducted based on [61], considering the FU of 1 ton of biomass input, and 1 GJ of biocoal output, which was followed due to the specific characteristics of each compared literature in Table 4. Since the literature in Table 7 has different boundary limits from this study, comparisons were made by specific process stages.

Zang et al. conducted LCA for various feedstocks (microalgae [21], spent coffee grounds [24], corn cob [22], and rice straw [23]). Their study considered the energy and carrier gas contributions from torrefaction experiments conducted at temperatures ranging from 200 to 300 °C, with varying residence times (15–60 min), for an FU of 1 ton of raw biomass input. Christoforou et al. [62], Tsalidis et al. [63], and Adams et al. [40] considered a broader system boundary, although they did not include combustion; therefore, the impact categories were presented in Table 7, both with and without the contribution of this stage.

Table 7 shows that the categories aligned (superscript “a” in Table 7) with the obtained results were $ADP_{fossil}$, AP, EP, GWP, HTP, and TETP across the referenced studies. Some categories in this study showed higher impacts (superscript “b” in Table 7), while others showed lower

**Table 4**
LCA average results compared with literature – harmonized per 1 ton of raw biomass input and 1 GJ of biocoal to the torrefaction process.

| **FU: 1 ton of biomass input** **Feedstock** | Study **UFW** | [21] **Microalgal** | [24] **SGC** | [22] **Corn cob** | [23] **Rice straw** |
|---|---|---|---|---|---|
| **ADP elements** | 3.00E-06 | – | 9.77E-02[b] | – | – |
| **ADP fossil** | 1.22E+02 | – | – | – | 6.80E-01[c] |
| **AP** | 9.00E-02 | 1.20E-01 [a] | – | – | – |
| **EP** | 1.00E-02 | 3.00E-02 [a] | – | – | – |
| **FAETP** | 1.50E-01 | 6.01E+00[b] | – | – | – |
| **GWP** [d] | 1.64E+03 | – | – | – | – |
| **GWP (energy and $N_2$)** [e] | 1.78E+04 | 1.69E+04 [a] | 1.31E+04 [a] | 2.00E-02[c] | 2.09E+04 [a] |
| **HTP** | 2.45E+00 | 1.75E+00 [a] | 2.06E+00 [a] | – | 2.21E+00 [a] |
| **MAETP** | 5.28E+03 | 2.12E+01[c] | – | – | – |
| **ODP** | 2.00E-10 | 2.53E-07[b] | 2.05E-07[b] | – | – |
| **POCP** | 4.09E-02 | 6.00E-04[c] | 6.00E-04[c] | – | – |
| **TETP** | 5.31E-02 | 1.80E-03[c] | 1.40E-03[c] | – | – |

| **FU: 1 GJ of biocoal** **Feedstock** | **Study** **UFW** | [20] **Rice husk pellets** | [63] **Wood pellets** | [40] **Wood pellets** |
|---|---|---|---|---|
| **ADP elements** | 1.00E-06 | – | – | – |
| **ADP fossil** | 4.01E+01 | 4.42E+01 [a] | – | – |
| **AP** | 9.00E-02 | 1.00E-01 [a] | – | – |
| **AP (without combustion)** [f] | 3.00E-02 | – | – | 2.00E-02 [a] |
| **EP** | 2.00E-02 | 1.70E-01[b] | – | – |
| **FAETP** | 4.90E-02 | – | 2.00E-03[c] | – |
| **GWP** * | 8.87E+01 | 4.33E+01[c] | – | – |
| **GWP (without combustion)** [f] | 6.50E+00 | – | 6.63E+00 [a] | 6.63E+00 [a] |
| **HTP** | 9.60E-01 | – | – | – |
| **MAETP** | 1.74E+03 | – | – | – |
| **ODP** | 1.00E-10 | 3.66E-06[b] | – | – |
| **POCP** | 1.00E-01 | – | – | – |
| **TETP** | 2.00E-02 | – | 2.00E-02 [a] | – |

[a] in-line, [b] higher, and [c] lower results compared to the literature. [d] The GWP values were presented considering only the positive emissions, excluding the negative emissions associated with $CO_2$ capture by feedstock. [e] The studies [21–24] focused only on the emissions from the torrefaction stage, considering energy use and carrier gas, but did not include emissions from the torgas. [f] The studies [20,40,63] did not consider the combustion of biocoal, and the categories that included the combustion stage presented results both with and without it. $ADP_{elements}$: Abiotic Depletion (elements) (kg Sb eq.); $ADP_{fossil}$: Abiotic Depletion (fossil) (MJ); AP: Acidification Potential (kg $SO_2$ eq.); EP: Eutrophication Potential (kg Phosphate eq.); FAETP: Freshwater Aquatic Ecotoxicity Potential (kg DCB eq.); GWP: Global Warming Potential (100 years) (kg $CO_2$ eq.); HTP: Human Toxicity Potential (kg DCB eq.); MAETP: Marine Aquatic Ecotoxicity Potential (kg DCB eq.); ODP: Ozone Layer Depletion Potential (steady state) (kg R11 eq.); POCP: Photochemical Ozone Creation Potential (kg Ethene eq.); TETP: Terrestrial Ecotoxicity Potential (kg DCB eq.).

impacts (superscript "c" in Table 7). This variation can be attributed to using the Brazilian energy matrix in the present study, whereas the referenced studies used energy systems from significantly different regions (Table 2). The most aligned category was GWP, while the others varied, either higher or lower, mainly depending on the energy matrix.

### 3.5. Global warming potential

An in-depth analysis of GWP was conducted to track the contribution of each process stage, considering the differences in defining FU (particularly mass-based). Fig. 6 illustrates the GWP analysis for the distinct stages of the system, namely feedstock ($CO_2$ uptake), drying, torrefaction, and combustion. The model equations in Table S11

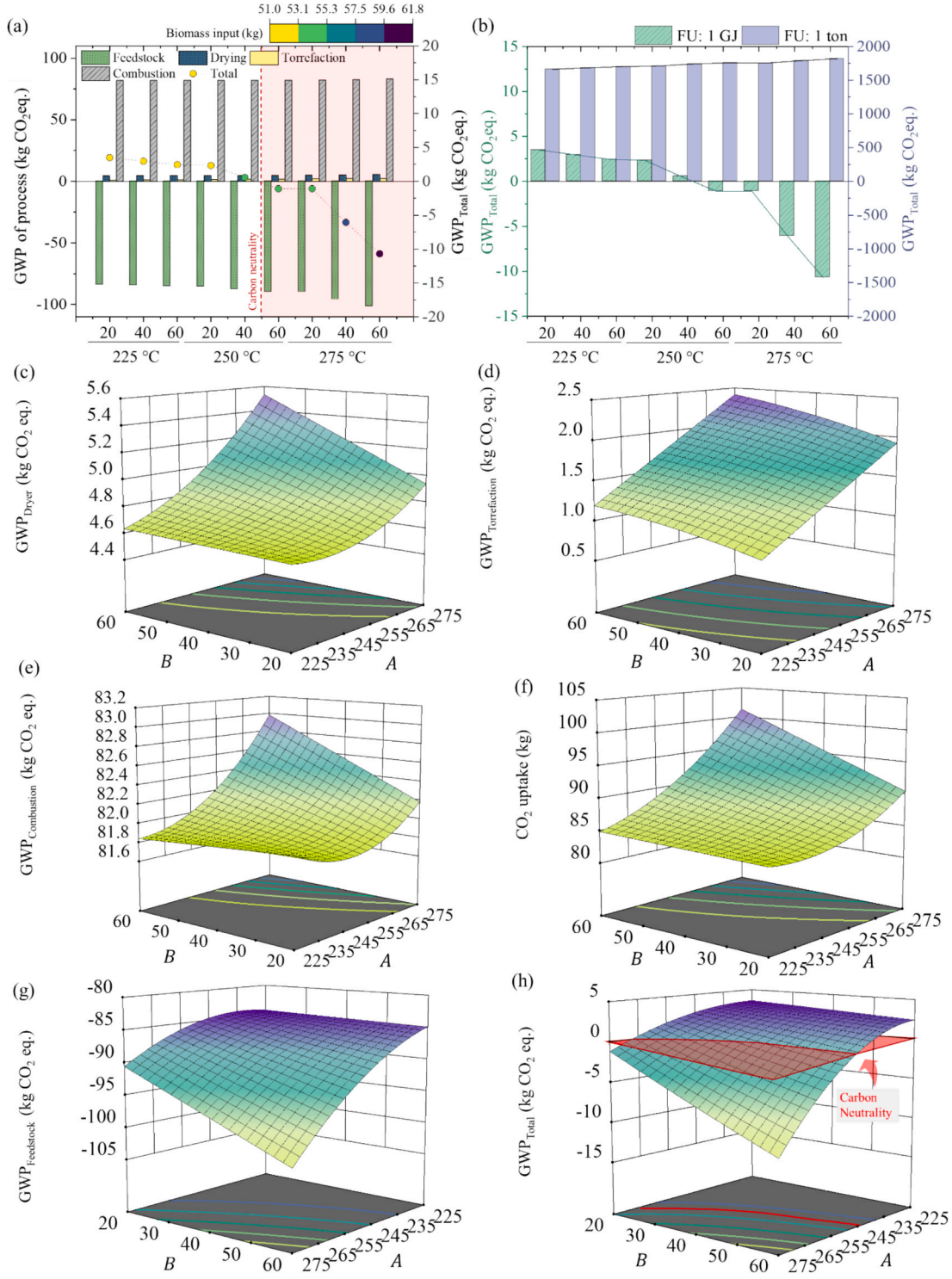


**Fig. 6.** (a) GWP for different stages of biomass processing, considering operational conditions and the contribution of different processes considering FU of 1GJ of biocoal output. (b) $GWP_{Total}$ considering the FU of 1 ton biocoal output and 1 GJ of biocoal output. 3D surface plots considering FU of 1 GJ of biocoal output showing the GWP as a function of operational parameters ($A$ – temperature in °C, and $B$ – time in min) for (c) $GWP_{Dryer}$, (d) $GWP_{Torrefaction}$, (e) $GWP_{Combustion}$, (f) $CO_2$ uptake, (g) $GWP_{Feedstock}$, and (h) $GWP_{Total}$ (sum of all processes stages), highlighting the carbon neutrality plan.

obtained the 3D surfaces in Fig. 6(c)–(h), which showcase reduced quadratic models for the $GWP_{Total}$ and each contribution (feedstock, dryer, torrefaction and combustion). The $GWP_{Total}$ ranges from positive to negative $CO_2$ emissions, demonstrating the carbon dynamics across different stages of the process (Fig. 6(a)). The processes themselves lead to positive emissions from the drying, torrefaction, and combustion stages, with average contributions to $GWP_{Total}$ of 6 %, 2 %, and 93 %, respectively (Fig. 6(c), (d), and (e)).

The GWP of the drying and combustion process (Fig. 6(c) and (d)) exhibits a pronounced temperature dependence, particularly between light and mild torrefaction (225–250 °C), with the importance of time dependency increasing at higher temperatures. The $GWP_{ryer}$ is directly tied to its energy requirements and is, therefore, intrinsically linked to the country's electricity grid where the plant is located. Meanwhile, the $GWP_{Combustion}$ stands for biocoal burning emissions ($CO_2$ and $CH_4$).

The $GWP_{Torrefaction}$ (Fig. 6(d)) is more temperature-driven and slightly dependent on treatment time, exhibiting the same trend across all operational conditions. The $GWP_{Torrefaction}$ is linked to the $CO_2$ emissions from the torgas released during treatment and the emissions related to the energy requirements (electric heating), thus also tied to the country's electricity grid mix.

In contrast, negative $GWP_{Feedstock}$ values (Fig. 6(g)) highlight the increasing contribution of $CO_2$ uptake by feedstock (Fig. 6(f)). This effect exhibits minimal time dependency during light torrefaction but becomes more pronounced with increased time and temperature under severe torrefaction conditions. As torrefaction intensifies, the greater amount of biomass input required (colormap in Fig. 6(a)) to attempt the 1 GJ of biocoal results in higher $CO_2$ uptake (Fig. 6(f)), thereby further reducing $GWP_{Feedstock}$ values and contributing to neutrality on $GWP_{Total}$ (Fig. 6(h)).

To better understand how environmental burdens are distributed among the output streams of the torrefaction process, Tables S20 and S21 present the allocation of GWP using energy-based and mass-based approaches. These methods reflect how impacts are attributed to biocoal, bio-oil, and torgas based on their respective lower heating values or dry mass fractions. When switching from energy-based to mass-based allocation, the average share of GWP attributed to biocoal decreases from 94.38 % to 89.05 %, while the share assigned to bio-oil increases from 5.49 % to 9.55 %, and to torgas from 0.13 % to 1.40 %. Given its composition and energy content, bio-oil has been investigated as a precursor for advanced biofuels and platform chemicals [39]. Its future valorization could play a significant role in enhancing carbon mitigation within integrated biomass utilization systems.

### 3.6. Carbon neutrality assessment

Fig. 6(h) shows the $GWP_{Total}$ (sum of all processes), presenting an analysis of carbon neutrality in the torrefaction process for FU of 1 GJ of biocoal. This surface is obtained through the RSM and described by the $GWP_{Total}$ equation in Table S11 of the SM. Since carbon neutrality is achieved when the total system's GWP equals zero, the intersection between the carbon neutrality plane ($GWP_{Total} = 0$) and the 3D surface representing $GWP_{Total}$ illustrates this condition (see Fig. 6(h)).

Below the carbon neutrality plane (in red), the associated temperatures and times indicate treatment conditions where the sum of all system components (feedstock, dryer, torrefaction, and combustion) corresponds to a carbon–neutral process. Above this plan, processes contribute to carbon emissions or global warming situations. This trend is also illustrated in Fig. 6(a), where the carbon neutrality line marks a clear decline in $GWP_{Total}$ as process severity increases.

The torrefaction neutrality equation (Eq. (13)) was derived by setting the total system's GWP ($GWP_{Total}$) equation (see Table S11) to zero, accounting for the contributions of each phase, carbon uptake, and applying an energy-based functional unit (1 GJ).

$$t = -1.61377023E-3 \times T^3 + 1.29779321 \times T^2 - 3.488334E2 \times T + 3.13582034E4 \quad (13)$$

This equation, represented by the red line in Fig. 6(h), determines the time ($t$, in min) and temperature ($T$, in °C) at which the GWP reaches zero, marking the point of carbon neutrality. It is important to note that this equation is valid for the assessed feedstock only within the specific temperature and time limits of 245.5–266.5 °C and 20–60 min. Notably, carbon neutrality can be achieved across all assessed treatment times (20–60 min); however, only a specific temperature range (245.5–266.5 °C) enabled this outcome. The assumptions and validation underlying this equation stem from each step of the framework, as the RSM was applied using input data from all prior analyses. Specifically, GWP depends on the feedstock properties, torrefaction reactor type and conditions, kinetic modeling, Aspen Plus process modeling, and LCA assumptions. These factors collectively define the validity of the equation within the studied torrefaction system.

While the proposed framework and modeling are theoretically capable of obtaining the equation for different biomass types and under alternative atmospheres (e.g., flue gas and $CO_2$), this would require a complete set of experimental data specific to those conditions, as lignocellulosic biomass is a complex and heterogeneous material with significant variations across different biomass types and decomposition behavior under different conditions.

What becomes evident from analyzing Fig. 6 is the importance of the FU definition on the LCA. An energy-based FU captures the intrinsic characteristics of the torrefaction process, the trade-off between biocoal yield reduction, its HHV enhancement and energy expenditures. In Fig. 6 (b), when a mass-based FU (1 ton) is defined, representing a fixed output amount of torrefied product (biocoal), a noticeable increase in GWP is revealed, driven by higher energy consumption as torrefaction severity increases. This trend is consistent with other impact categories (Table S18) and aligns with microalga [21] and rice straw [23] torrefaction, which consider the FU based on mass.

Defining an energy-based FU accounts for the trade-off between energy consumption, biocoal yield, and the increase in HHV. Higher torrefaction severity results in greater mass loss, but it simultaneously produces biocoal with improved energy quality (HHV). Even with an HHV enhancement of biocoal, this mass loss reflects on a higher input of raw biomass to achieve the same functional unit of 1 GJ (biocoal energy) output. Consequently, the increased biomass input leads to greater $CO_2$ uptake. This influence is further visualized in Fig. 6(a), which presents the $GWP_{Total}$ trend and a color map that indicates the amount of biomass input required, considering the FU of 1 GJ of biocoal. The red area in the figure marks where $CO_2$ uptake by the feedstock exceeds the GHG emissions from the entire production process, demonstrating the potential for net carbon sequestration under specific conditions.

For example, in Fig. 6(a), at 250 °C for 40 min (before reaching the carbon neutrality line), the $GWP_{Total}$ is 0.58 kg $CO_2$ eq.. The feedstock contributes –87.84 kg $CO_2$ eq. through carbon sequestration. Meanwhile, the combined dryer, torrefaction, and combustor emissions amount to 88.42 kg $CO_2$ eq. In contrast, at 250 °C for 60 min, the process results in a negative $GWP_{Total}$ of –1.09 kg $CO_2$ eq., with the feedstock sequestering –89.88 kg $CO_2$ eq., offsetting emissions from other stages (88.78 kg $CO_2$ eq.), and leading to a net carbon capture scenario. Other runs follow similar patterns, with the $CO_2$ uptake from feedstock playing a key role in balancing $CO_2$ emissions, sometimes even yielding negative $GWP_{Total}$ depending on process conditions (Fig. 6(a) and (h)). These results show the importance of FU and system boundary definitions.

Another important aspect of understanding the GWP dynamics is evaluating the bio-oil yield (Fig. 2(e)). As the torrefaction severity increases, the bio-oil yields are higher (around 20 %). When properly conditioned, this by-product acts as a carbon stock, as it does not undergo combustion and can be applied to several further applications [64].

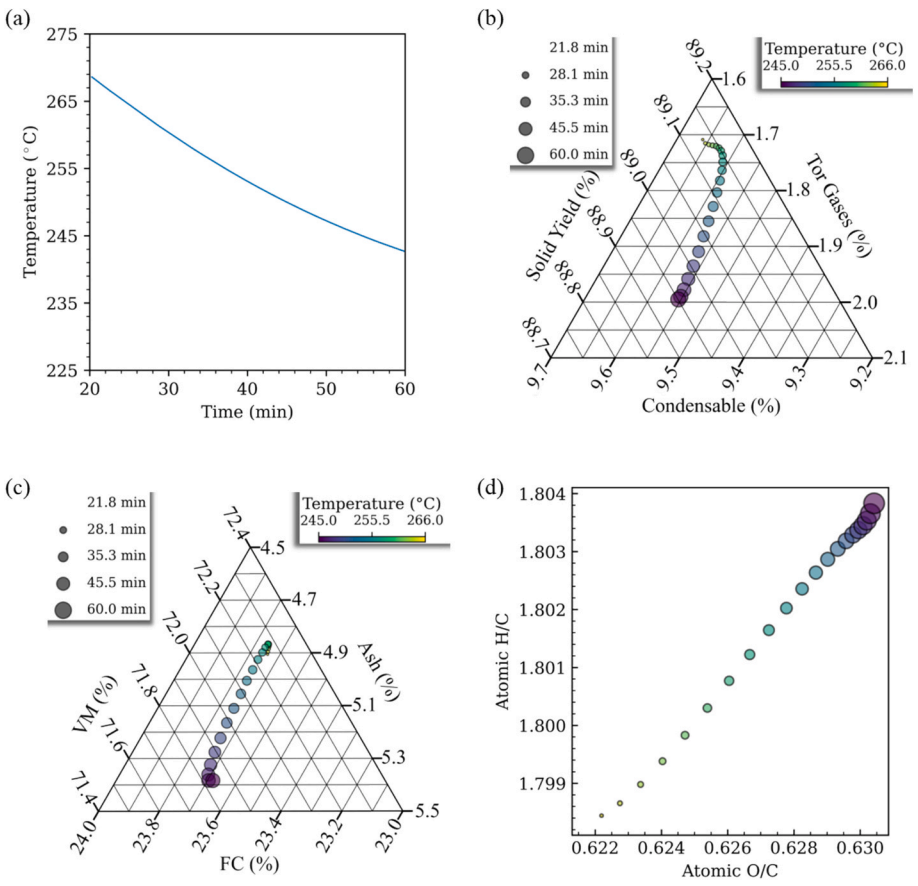


**Fig. 7.** (a) Carbon neutrality (GWP = 0) analysis as a function of temperature and time in the torrefaction process. (b) Biocoal, bio-oil, and torgas yields as a function of time and temperature, (c) Proximate properties (volatile matter, fixed carbon, and ash content) across different conditions, and (d) Correlation between hydrogen-to-carbon (H/C) and oxygen-to-carbon (O/C) ratios as temperature and time vary along the carbon neutrality line.

Fig. 7 illustrates a carbon neutrality (GWP = 0) analysis for the properties of the obtained biocoal within the specific temperature and time conditions of carbon neutrality (245.5–266.5 °C and 20–60 min). In addition, Table S22 presents the tabulated values.

Fig. 7 reveals that it is possible to maintain similar properties along the GWP = 0 (carbon neutrality) line by adjusting temperature and time within the identified ranges (Fig. 7 (a)), with only minor variations in key parameters. The biocoal yield, for instance, slightly varied from

**Table 5**
Predicted, observed and error values of responses at optimal torrefaction conditions.

| **Parameters** | | | | | | **Goal** |
|---|---|---|---|---|---|---|
| *A*: Temperature | | 256.17 °C | | | | **in range** |
| *B*: Time | | 41.01 min | | | | **in range** |
| **Responses** | **Model** | **Standard deviation** | **95 % PI low** | **Observed** | **95 % PI high** | |
| **Biocoal quality** | | | | | | |
| Biocoal SY | 87.82 | 0.39 | 86.87 | 87.85 | 88.77 | maximize |
| ASH | 4.98 | 0.01 | 4.95 | 4.98 | 5.02 | minimize |
| FR | 0.34 | 0 | 0.33 | 0.34 | 0.35 | maximize |
| $HHV_{biocoal}$ | 20.98 | 0.02 | 20.94 | 20.97 | 21.03 | maximize |
| **Process efficiency** | | | | | | |
| Irreversibility | 8.15E+04 | 4.38E+03 | 6.99E+04 | 7.70E+04 | 9.30E+04 | minimize |
| **Environmental impacts** | | | | | | |
| $GWP_{Total}$ | −5.04E-01 | 5.66E-02 | −6.75E-01 | −6.32E-01 | −3.33E-01 | minimize |
| ADP elements | 1.04E-06 | 8.07E-09 | 1.02E-06 | 1.05E-06 | 1.06E-06 | minimize |
| ADP fossil | 4.00E+01 | 3.10E-01 | 3.92E+01 | 4.02E+01 | 4.08E+01 | minimize |
| AP | 9.16E-02 | 5.51E-04 | 9.01E-02 | 9.13E-02 | 9.30E-02 | minimize |
| EP | 1.97E-02 | 1.11E-04 | 1.94E-02 | 1.96E-02 | 2.00E-02 | minimize |
| FAETP | 4.84E-02 | 3.75E-04 | 4.74E-02 | 4.86E-02 | 4.94E-02 | minimize |
| HT | 9.61E-01 | 7.01E-03 | 9.44E-01 | 9.58E-01 | 9.78E-01 | minimize |
| MAEP | 1.75E+03 | 1.34E+01 | 1.72E+03 | 1.74E+03 | 1.78E+03 | minimize |
| OLDP | 5.11E-11 | 3.93E-13 | 5.02E-11 | 5.10E-11 | 5.21E-11 | minimize |
| POCP | 9.82E-02 | 7.13E-05 | 9.80E-02 | 9.81E-02 | 9.84E-02 | minimize |
| TETP | 1.76E-02 | 1.35E-04 | 1.73E-02 | 1.75E-02 | 1.79E-02 | minimize |
| **Desirability** | 0.526 | | | | | |

88.68 % to 89.09 % as the temperature rises from 245.5 °C to 266.5 °C and time decreases from 60 to 20 min. Simultaneously, bio-oil and torgas yields show marginal decreases, highlighting that higher temperatures and shorter times favor biocoal recovery without significantly impacting volatile by-products. Considering the carbon neutrality line (GWP = 0), the bio-oil yield ranges between 0.35 % and 11.36 % (Fig. 7 (b) and Table S22) within the carbon neutrality line.

Proximate properties, such as volatile matter and ash content, exhibit minimal changes across the range of carbon neutrality. Thus, it suggests that temperature and time can be adjusted within the defined limits to maintain consistent biomass proximate properties while achieving carbon neutrality. The H/C and O/C ratios also show slight adjustments, indicating a shift toward a more carbon-rich composition at higher temperatures and shorter times, which is beneficial for enhancing fuel properties.

This flexibility enables the use of various technologies with inherent limitations in terms of temperature or time control. Adjusting these parameters within the narrow range where carbon neutrality is maintained allows for accommodating different process constraints while still optimizing the biofuel's properties. This adaptability ensures that even systems with restricted operational capacities can still produce high-quality biocoal with minimized environmental impact.

### 3.7. Torrefaction optimization

Table 5 presents the predicted, observed, and error values for the optimized responses. Table S23 in SM complements Table 8, presenting all 30 responses for the optimal condition. Additionally, Fig. 8 presents the surface of the desirability function and Sankey diagrams for the optimal process's mass, energy, and carbon flow, obtained at 256.17 °C and 41.01 min. The zero values for desirability result from the $GWP_{Total}$ being constrained to be less than zero through optimization, which considers only carbon–neutral or negative torrefaction conditions.

The observed data demonstrates high alignment with the predicted values, as evidenced by the narrow standard deviations (SD) and 95 % prediction intervals (PI) (Table 8). For instance, the biocoal yield shows a slight deviation between predicted (87.82 %) and observed (87.85 %) values, with a very narrow 95 % PI (86.87–88.77 %), indicating strong model reliability. Ash content was minimized at 4.98 %. The fuel ratio of 0.34 and HHV of 20.98 MJ $kg^{-1}$ indicate a high energy content and combustibility, making the biocoal suitable for energy production. Ash, FR and HHV exhibit low standard deviations (0.01, 0, and 0.02, respectively), confirming the precision of the model.

SY: Solid Yield (%). ASH (%). FR: Fuel Ratio (dimensionless); $HHV_{biocoal}$: Higher Heating Value (MJ $kg^{-1}$); Irreversibility (kJ $h^{-1}$);

Reduced system irreversibility to 8.15E+04 MJ enhances process efficiency, lowering energy losses during conversion. Environmental

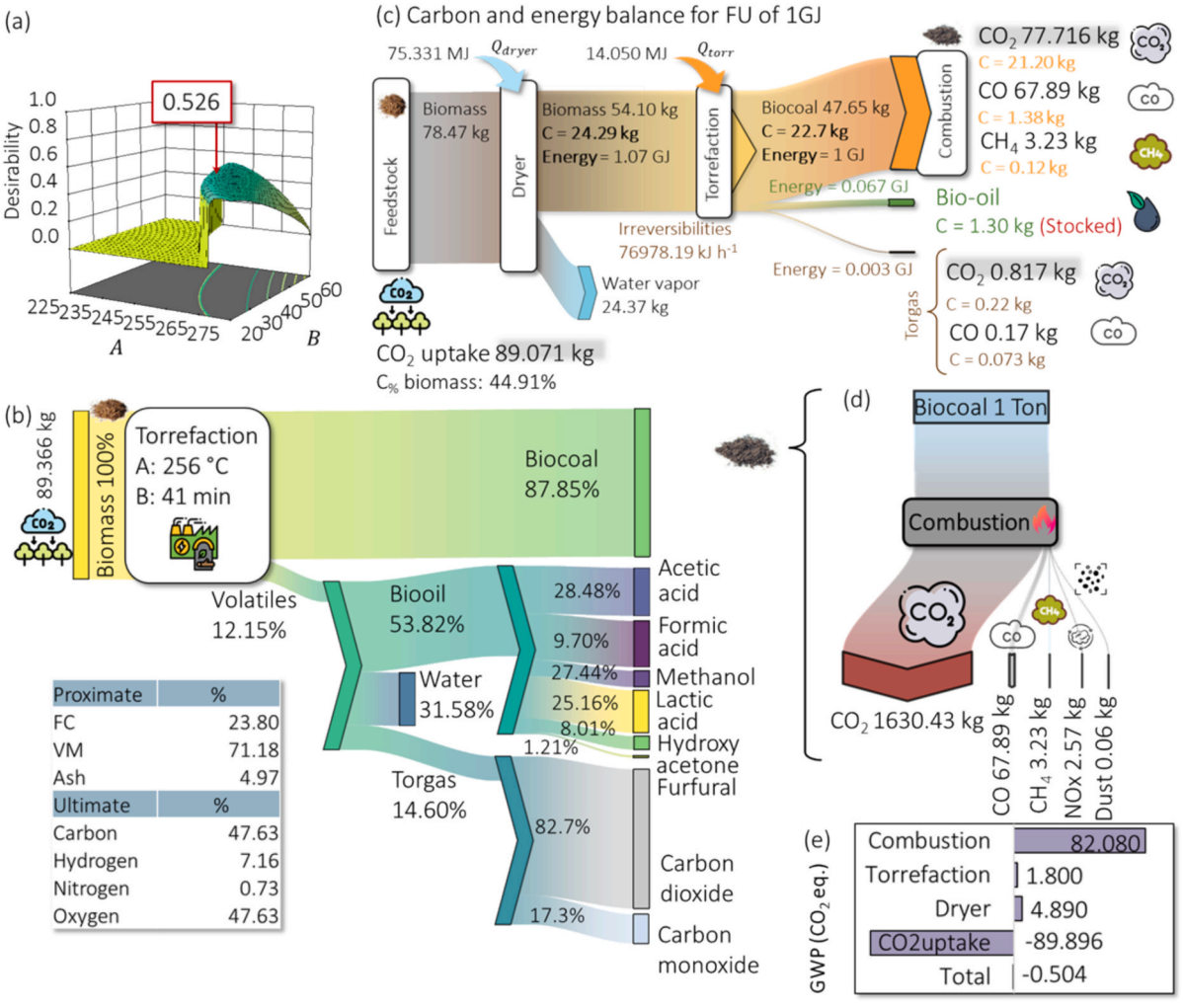


**Fig. 8.** (a) Optimization of the desirability surface (for torrefaction temperature (*A* in °C) and times (*B* in min)). (b) Sankey diagram illustrates the mass balance, torrefaction irreversibilities and the ultimate and proximate properties of the biocoal. (c) Carbon and energy balance considering the FU of 1 GJ. (d) Sankey diagram detailing combustion emissions of 1 ton of biocoal produced at optimal condition. (e) Global Warming Potential (GWP) analysis of the processes' contributions considering the optimal solution.

impacts, particularly GWP, are minimized, with a net reduction in carbon emissions (–0.504 kg $CO_2$ eq.), emphasizing carbon neutrality. Carbon sequestration in the feedstock (–89.896 kg $CO_2$ eq.) plays a significant role. Abiotic depletion, acidification, eutrophication, and toxicity potentials are also reduced, enhancing the process's sustainability. The irreversibility and environmental impacts also exhibit tight prediction intervals, further reinforcing the model's accuracy in minimizing process inefficiencies and environmental impacts. The overall low errors between predicted and observed values and consistent standard deviations suggest that the optimization process is highly reliable and can deliver consistent, high-quality outcomes for torrefaction conditions.

Table S24 compares prior works that evaluate the optimization of torrefaction treatment using RSM. The optimal conditions vary among feedstocks, reflecting the impact of temperature and time on biocoal yield and quality. The diversity in feedstock characteristics highlights the importance of tailoring torrefaction conditions to achieve desired outcomes, whether focusing on high biocoal yield, energy yield, reduced emissions, or carbon retention. Feedstocks like microalgae provide practical options for low-temperature torrefaction, UFW at mild severities, while agricultural residues, such as corncob, are optimized at high severities. When selecting biomass sources for sustainable biofuel production, the unique properties of each feedstock and its optimal conditions should be considered, with implications for industrial energy recovery and reduced environmental impact.

## 4. Limitations and prospects

This study identifies limitations in the two-step model, which, while simplifying reaction pathways, overlooks biomass variability, secondary reactions, and scale-up challenges, including heat and mass transfer dynamics. Another critical limitation is the assumption of a fixed volatile composition, which reduces the accuracy of $CO_2$ emission and bio-oil yield predictions. Advanced techniques, such as Py-GC/MS, should be used to characterize volatiles [65], while cone calorimetry can support the analysis of combustion behavior under controlled conditions [65]. Additionally, the combustion gas composition of torrefied biomass remains poorly documented, necessitating further research using GC–MS for precise emission quantification [66]. Importantly, the results are specific to the studied UFW blend, which is composed of hardwood species with relatively uniform characteristics; therefore, extrapolation to other biomass types requires further empirical validation. Instead of pursuing a universal model, future work should generate robust datasets for specific biomasses under controlled conditions. Artificial intelligence and machine learning [67] can then integrate these data to develop predictive tools that improve process adaptability and support biomass-to-fuel decision-making.

At an industrial scale, gas–solid interactions and residence time become difficult to control. Contrary to the model's assumption of uniform heating, practical factors such as feedstock heterogeneity, particle size, and reactor design affect process efficiency. Industrial reactors also exhibit greater thermal gradients, resulting in uneven heating and reduced product uniformity. Accurate scale-up requires improved heat transfer modeling and pilot-scale validation across different reactor types, feedstocks, and operational conditions. Additionally, industrial implementations may adopt flue gas or $CO_2$-rich atmospheres, which can influence energy efficiency and environmental outcomes.

An often overlooked factor is the environmental impact of urban forestry operations, including planting, maintenance, pruning, and transportation. These upstream activities should be incorporated into future LCAs to enhance accuracy. Literature reports GWP from such activities ranging from 0.0157 to 0.0709 kg $CO_2$ eq. $kg^{-1}$ [68], which are lower than drying emissions and substantially lower than those from biocoal combustion. While relatively modest, these contributions become more relevant under mass-based functional units, whereas their influence varies under energy-based units depending on conversion severity. Moreover, although a standard $CO_2$ uptake method was applied, a tailored approach specific to urban pruning residues would improve sequestration estimates. Lastly, this study did not explore mitigation strategies such as gas re-circulation [2], BECCS, enhanced $CO_2$ sequestration, or carbon capture systems [69]. Future research should evaluate these technologies to determine their viability in reducing emissions while maintaining or improving energy performance in carbon–neutral biofuel production.

## 5. Conclusions

This study presents a novel integration of biocoal quality, energy efficiency, and potential environmental impact into a unified framework for torrefaction optimization using response surface methodology. By modeling the process thermodynamically and environmentally, the approach overcomes the limitations of single-objective models and provides a robust tool for sustainable biomass valorization. Optimal conditions (256.17 °C, 41.01 min) yielded high-quality biocoal (HHV = 20.98 MJ $kg^{-1}$, FR = 0.34, ash = 4.98 %) with 87.82 % solid yield and net carbon sequestration of –0.504 kg $CO_2$ eq. per GJ of biocoal. These findings confirm the potential for carbon-negative energy solutions. The integration of LCA into the optimization process revealed critical trade-offs and introduced a new equation defining the carbon neutrality boundary (245.5–266.5 °C; 20–60 min). This equation is applicable within the defined experimental domain and specific feedstock, supporting scenario-specific evaluation. This approach enhances decision-making by linking process efficiency with environmental targets and enabling flexible adjustment of operational parameters to meet quality or sustainability goals. Overall, the framework contributes to advancing torrefaction as a scalable and climate-aligned bioenergy pathway.

**Acknowledgement and Funding**

The research presented was supported by the Brazilian National Council for Scientific and Technological Development (CNPq – process no. 406053/2022–7, 304165/2022–0 and 305109/2023–5), Coordination for the Improvement of Higher Education Personnel (CAPES) – Finance Code 001, Brazilian Forest Products Laboratory (LPF), Decanato de Pesquisa e Inovação (DPI/UnB, and Federal District Research Foundation (FAPDF – Project 469/2023, Grant Term N°.00193–00002254/2023–19) and Fundação de Amparo à Pesquisa do Estado de Minas Gerais – FAPEMIG (FAPEMIG/DPE Grant Term No. 103658065/2024, Process: APQ-05431-24).

## CRediT authorship contribution statement

**Giulia Cruz Lamas:** Writing – review & editing, Writing – original draft, Visualization, Validation, Methodology, Investigation, Formal analysis, Data curation, Conceptualization. **Thiago da Silva Gonzales:** Writing – review & editing, Writing – original draft, Validation, Methodology, Investigation, Formal analysis, Data curation, Conceptualization. **Simone Monteiro:** Writing – review & editing, Validation, Supervision, Software, Formal analysis. **Pedro Paulo de Oliveira Rodrigues:** Writing – review & editing, Visualization, Software, Formal analysis. **Lucélia A. Macedo:** Writing – review & editing, Resources. **Thiago O. Rodrigues:** Writing – review & editing, Validation. **Patrick Rousset:** Writing – review & editing. **Thiago de Paula Protásio:** Writing – review & editing. **Armando Caldeira Pires:** Writing – review & editing. **Edgar A. Silveira:** Writing – review & editing.

## Declaration of competing interest

The authors declare that they have no known competing financial interests or personal relationships that could have appeared to influence the work reported in this paper.

## Appendix A. Supplementary data

Supplementary data to this article can be found online at https://doi.org/10.1016/j.enconman.2025.120055.

## Data availability

Data will be made available on request.

## References


[1] Sulis DB, Lavoine N, Sederoff H, Jiang X, Marques BM, Lan K, et al. Advances in lignocellulosic feedstocks for bioenergy and bioproducts. Nat Commun 2025;16:1244. https://doi.org/10.1038/s41467-025-56472-y.

[2] Thengane SK, Kung KS, Gomez-Barea A, Ghoniem AF. Advances in biomass torrefaction: Parameters, models, reactors, applications, deployment, and market. Prog Energy Combust Sci 2022;93:101040. https://doi.org/10.1016/j.pecs.2022.101040.

[3] dos Santos EV, Soares ÁAV, Rabêlo FHS, Silva SHG, Lima MDR, Bufalino L, et al. Effects of Fertilization, Soil Texture, and Forking on the Wood Quality and Yield of Energy Plantations of Tachigali vulgaris in Amazonia. Bioenergy Res 2025;18. https://doi.org/10.1007/s12155-025-10828-w.

[4] da Silva T, Carvalho N, Silveira EA, de Paula PT, Mendoza-Martinez C, Bianchi ML, et al. Optimizing Catalytic Hydrothermal Carbonization of Eucalyptus grandis Sawdust for Enhanced Biomass Energy Production: Statistical Analysis and Insights of Sustainable Carbon-Neutral Pathways. Energy 2025:134647. https://doi.org/10.1016/j.energy.2025.134647.

[5] Ong HC, Yu KL, Chen W-H-H, Pillejera MK, Bi X, Tran K-Q-Q, et al. Variation of lignocellulosic biomass structure from torrefaction: A critical review. Renewable and Sustainable Energy Reviews 2021;152:111698. https://doi.org/10.1016/j.rser.2021.111698.

[6] Chen W-H, Peng J, Bi XT. A state-of-the-art review of biomass torrefaction, densification and applications. Renewable and Sustainable Energy Reviews 2015;44:847–66. https://doi.org/10.1016/j.rser.2014.12.039.

[7] Pawlak-Kruczek H, Arora A, Gupta A, Saeed MA, Niedzwiecki L, Andrews G, et al. Biocoal - Quality control and assurance. Biomass Bioenergy 2020;135. https://doi.org/10.1016/j.biombioe.2020.105509.

[8] Yek PNY, Cheng YW, Liew RK, Wan Mahari WA, Ong HC, Chen W-H, et al. Progress in the torrefaction technology for upgrading oil palm wastes to energy-dense biochar: A review. Renewable and Sustainable Energy Reviews 2021;151:111645. https://doi.org/10.1016/j.rser.2021.111645.

[9] Barbosa T, Sant'Anna Chaves B, Gustavo O. Galvão L, Cruz Lamas G, Paulo de Oliveira Rodrigues P, Gabi Moreira M, et al. Waste-to-energy in the civil-construction sector toward the valuation of wood construction residues: Integration of torrefaction process. Fuel 2024;371. doi: 10.1016/j.fuel.2024.132029.

[10] Thengane SK, Burek J, Kung KS, Ghoniem AF, Sanchez DL. Life cycle assessment of rice husk torrefaction and prospects for decentralized facilities at rice mills. J Clean Prod 2020;275:123177. https://doi.org/10.1016/j.jclepro.2020.123177.

[11] Gizaw DG, Periyasamy S, Baylie H, Tassew Redda Z, Asaithambi P, Jayakumar M, et al. Advances in solid biofuels production through torrefaction: Potential biomass, types of torrefaction and reactors, influencing process parameters and future opportunities – A review. Process Safety and Environmental Protection 2024;186:1307–19. https://doi.org/10.1016/j.psep.2024.04.070.

[12] Mukherjee A, Okolie JA, Niu C, Dalai AK. Experimental and Modeling Studies of Torrefaction of Spent Coffee Grounds and Coffee Husk: Effects on Surface Chemistry and Carbon Dioxide Capture Performance. ACS Omega 2022;7:638–53. https://doi.org/10.1021/acsomega.1c05270.

[13] Kota KB, Shenbagaraj S, Sharma PK, Sharma AK, Ghodke PK, Chen WH. Biomass torrefaction: An overview of process and technology assessment based on global readiness level. Fuel 2022;324. https://doi.org/10.1016/j.fuel.2022.124663.

[14] Silveira EA, Santanna Chaves B, Macedo L, Ghesti GF, Evaristo RBW, Cruz Lamas G, et al. A hybrid optimization approach towards energy recovery from torrefied waste blends. Renew Energy 2023;212:151–65. https://doi.org/10.1016/j.renene.2023.05.053.

[15] Onsree T, Jaroenkhasemmeesuk C, Tippayawong N. Techno-economic assessment of a biomass torrefaction plant for pelletized agro-residues with flue gas as a main heat source. Energy Reports 2020;6:92–6. https://doi.org/10.1016/j.egyr.2020.10.043.

[16] Manouchehrinejad M, Mani S. Process simulation of an integrated biomass torrefaction and pelletization (iBTP) plant to produce solid biofuels. Energy Conversion and Management: X 2019;1. https://doi.org/10.1016/j.ecmx.2019.100008.

[17] Arteaga-Pérez LE, Segura C, Espinoza D, Radovic LR, Jiménez R. Torrefaction of Pinus radiata and Eucalyptus globulus: A combined experimental and modeling approach to process synthesis. Energy for Sustainable Development 2015;29:13–23. https://doi.org/10.1016/J.ESD.2015.08.004.

[18] Bach QV, Skreiberg Ø, Lee CJ. Process modeling for torrefaction of birch branches. Energy Procedia 2017;142:395–400. https://doi.org/10.1016/J.EGYPRO.2017.12.062.

[19] Sukpancharoen S, Sirimongkol R, Khojitmate S, Rattanachoung N, Junhuathon N, Phetyim N. Simulation and Optimization of High Heating Value for Rice Husk Biomass in Torrefaction Process. Lecture Notes. Electrical Engineering 2023;1058 LNEE:301–13. https://doi.org/10.1007/978-981-99-3888-9_22.

[20] Thengane SK, Burek J, Kung KS, Ghoniem AF, Sanchez DL. Life cycle assessment of rice husk torrefaction and prospects for decentralized facilities at rice mills. J Clean Prod 2020;275. https://doi.org/10.1016/j.jclepro.2020.123177.

[21] Zhang C, Wang M, Chen WH, Pétrissans A, Pétrissans M, Ho SH. A comparison of conventional and oxidative torrefaction of microalga Nannochloropsis Oceanica through energy efficiency analysis and life cycle assessment. J Clean Prod 2022;369. https://doi.org/10.1016/j.jclepro.2022.133236.

[22] Zhang C, Chen WH, Ho SH. Elemental loss, enrichment, transformation and life cycle assessment of torrefied corncob. Energy 2022;242. https://doi.org/10.1016/j.energy.2021.123019.

[23] Zhang C, Yang W, Chen WH, Ho SH, Pétrissans A, Pétrissans M. Effect of torrefaction on the structure and reactivity of rice straw as well as life cycle assessment of torrefaction process. Energy 2022;240. https://doi.org/10.1016/j.energy.2021.122470.

[24] Zhang C, Chen WH, Ho SH. Economic feasibility analysis and environmental impact assessment for the comparison of conventional and microwave torrefaction of spent coffee grounds. Biomass Bioenergy 2023;168:106652. https://doi.org/10.1016/j.biombioe.2022.106652.

[25] Bispo LFP, Nolasco AM, de Souza EC, Klingenberg D, Dias Júnior AF. Valorizing urban forestry waste through the manufacture of toys. Waste Management 2021;126:351–9. https://doi.org/10.1016/J.WASMAN.2021.03.028.

[26] Governo do Distrito Federal. PDGIRS – Plano Distrital De Gestão Integrada De Resíduos Sólidos. vol. 3. Brasília - DF: Governo do Distrito Federal; 2018.

[27] Silveira EA, Santanna MS, Barbosa Souto NP, Lamas GC, Galvão LGO, Luz SM, et al. Urban lignocellulosic waste as biofuel: thermal improvement and torrefaction kinetics. J Therm Anal Calorim 2023. https://doi.org/10.1007/s10973-022-11515-0.

[28] Gonzales T da S, Rodrigues PP de O, Lamas GC, Moreira MG, Barcelo R, Silva SM e, et al. A Process Modeling and Simulation Study for Forest Urban Waste Torrefaction. 31 European Biomass Conference & Exhibition, 2023, p. 0–6. doi: 10.5071/31stEUBCE2023-5BV.10.7.

[29] Di Blasi C, Lanzetta M. Intrinsic kinetics of isothermal xylan degradation in inert atmosphere. J Anal Appl Pyrolysis 1997;40–41:287–303. https://doi.org/10.1016/S0165-2370(97)00028-4.

[30] Bates RB, Ghoniem AF. Biomass torrefaction: Modeling of volatile and solid product evolution kinetics. Bioresour Technol 2012;124:460–9. https://doi.org/10.1016/j.biortech.2012.07.018.

[31] Prins MJ, Ptasinski KJ, Janssen FJJGJG. Torrefaction of wood. Part 1. Weight loss kinetics. J Anal Appl Pyrolysis 2006;77:28–34. https://doi.org/10.1016/j.jaap.2006.01.002.

[32] Chai M, Xie L, Yu X, Zhang X, Yang Y, Rahman MM, et al. Poplar wood torrefaction: Kinetics, thermochemistry and implications. Renewable and Sustainable Energy Reviews 2021;143. https://doi.org/10.1016/j.rser.2021.110962.

[33] Gonzales T da S, Monteiro S, Lamas GC, Rodrigues PPO, Siqueira MBB, Follegatti-Romero LA, et al. Simulation and Thermodynamic Evaluation of Woody Biomass Waste Torrefaction. ACS Omega 2025;10:3585–97. doi: 10.1021/acsomega.4c08299.

[34] Singh RK, Jena K, Chakraborty JP, Sarkar A. Energy and exergy analysis for torrefaction of pigeon pea stalk (cajanus cajan) and eucalyptus (eucalyptus tereticornis). Int J Hydrogen Energy 2020;45:18922–36. https://doi.org/10.1016/J.IJHYDENE.2020.05.045.

[35] Song G, Shen L, Xiao J. Estimating specific chemical exergy of biomass from basic analysis data. Ind Eng Chem Res 2011;50:9758–66. https://doi.org/10.1021/IE200534N.

[36] Gu Z, Liu Z, Yang S, Xie N, Ma K. Exergy and environmental footprint analysis for a green ammonia production process. J Clean Prod 2024;455. https://doi.org/10.1016/j.jclepro.2024.142357.

[37] Ling JLJ, Park HS, Lee HE, Solanki BS, Lee SH. Thermodynamic and exergy assessment of a biomass oxy-fuel combustion with supercritical carbon dioxide cycle under various recycle flue gas conditions. J Clean Prod 2024;458. https://doi.org/10.1016/j.jclepro.2024.142516.

[38] Ro JW, Zhang Y, Kendall A. Developing guidelines for waste designation of biofuel feedstocks in carbon footprints and life cycle assessment. Sustain Prod Consum 2023;37:320–30. https://doi.org/10.1016/j.spc.2023.03.009.

[39] Royko MM, Drummond SM, Boyt J, Ghoreishian SM, Lauterbach J. Novel process for the upgrading of model torrefaction bio-oils using ammonia. Front Energy Res 2022;10. https://doi.org/10.3389/fenrg.2022.1088902.

[40] Adams PWR, Shirley JEJ, McManus MC. Comparative cradle-to-gate life cycle assessment of wood pellet production with torrefaction. Appl Energy 2015;138:367–80. https://doi.org/10.1016/j.apenergy.2014.11.002.

[41] Silveira EA, Caldeira-Pires A, Luz SM, Silveira CM. Mass and energy allocation method analysis for an oil refinery characterization using multi-scale modeling. Int J Life Cycle Assess 2017;22:1815–22. https://doi.org/10.1007/s11367-017-1369-9.

[42] Moreira MG, Paulo P, Rodrigues O, Fernanda L, Garcia A, Lamas GC, et al. Assessment of wood residue blends from the amazon region for decentralized energy recovery and decarbonization: Combustion kinetics, thermodynamics and potential emissions including those for text and data mining, AI training, and similar technologies. Biomass Bioenergy 2025;197:107827. https://doi.org/10.1016/j.biombioe.2025.107827.

[43] Ozgen S, Cernuschi S, Caserini S. An overview of nitrogen oxides emissions from biomass combustion for domestic heat production. Renewable and Sustainable Energy Reviews 2021;135. https://doi.org/10.1016/j.rser.2020.110113.

[44] Maj G. Emission factors and energy properties of agro and forest biomass in aspect of sustainability of energy sector. Energies (Basel) 2018;11. https://doi.org/10.3390/en11061516.
[45] Maj G, Najda A, Klimek K, Balant S. Estimation of energy and emissions properties of waste from various species of mint in the herbal products industry. Energies (Basel) 2019;13. https://doi.org/10.3390/en13010055.
[46] Singh RK, Chakraborty JP, Sarkar A. Optimizing the torrefaction of pigeon pea stalk (cajanus cajan) using response surface methodology (RSM) and characterization of solid, liquid and gaseous products. Renew Energy 2020;155:677–90. https://doi.org/10.1016/j.renene.2020.03.184.
[47] Ozonoh M, Oboirien BO, Daramola MO. Optimization of process variables during torrefaction of coal/biomass/waste tyre blends: Application of artificial neural network & response surface methodology. Biomass Bioenergy 2020;143:105808. https://doi.org/10.1016/j.biombioe.2020.105808.
[48] Mendonça IF, do Vale GS, Evaristo RBW, Dutra RC, Paulo de Oliveira Rodrigues P, Silveira EA, et al. Optimizing torrefaction of banana waste (peels and rachis) for sustainable biocoal production in rural communities. Biomass Bioenergy 2025;196. doi: 10.1016/j.biombioe.2025.107726.
[49] Martínez MG, Couce AA, Dupont C, da Silva PD, Thiéry S, Meyer X, et al. Torrefaction of cellulose, hemicelluloses and lignin extracted from woody and agricultural biomass in TGA-GC/MS: Linking production profiles of volatile species to biomass type and macromolecular composition. Ind Crops Prod 2022;176:114350.
[50] Chen W-H, Lin B-J, Lin Y-Y, Chu Y-S, Ubando AT, Show PL, et al. Progress in biomass torrefaction: Principles, applications and challenges. Prog Energy Combust Sci 2021;82:100887. https://doi.org/10.1016/j.pecs.2020.100887.
[51] Prins MJ, Ptasinski KJ, Janssen FJJG. Torrefaction of wood: Part 2. Analysis of products. J Anal Appl Pyrolysis 2006;77:35–40. https://doi.org/10.1016/j.jaap.2006.01.001.
[52] Demirbas A. The influence of temperature on the yields of compounds existing in bio-oils obtained from biomass samples via pyrolysis. Fuel Processing Technology 2007;88:591–7. https://doi.org/10.1016/j.fuproc.2007.01.010.
[53] Nocquet T, Dupont C, Commandre JM, Grateau M, Thiery S, Salvador S. Volatile species release during torrefaction of wood and its macromolecular constituents: Part 1 - Experimental study. Energy 2014;72:180–7. https://doi.org/10.1016/j.energy.2014.02.061.
[54] Batista jan.. Torrefação do Pinus elliottii para fins energéticos. Unessp 2015.
[55] Arias B, Pevida C, Fermoso J, Plaza MGG, Rubiera F, Pis JJJ. Influence of torrefaction on the grindability and reactivity of woody biomass. Fuel Processing Technology 2008;89:169–75. https://doi.org/10.1016/j.fuproc.2007.09.002.
[56] Lima MDR, Simetti R, Assis MR de, Trugilho PF, Carneiro A de CO, Bufalino L, et al. Charcoal of logging wastes from sustainable forest management for industrial and domestic uses in the Brazilian Amazonia. Biomass Bioenergy 2020;142. doi: 10.1016/j.biombioe.2020.105804.
[57] Silveira EA, Lamas GC, de O. Rodrigues PP, Souto NPB, Sant'Anna Chaves B, Oliveira Galvão LG, et al. Effect of torrefaction severity on the energy recovery from amazonian wood residues for decentralized energy conversion systems. Biomass Bioenergy 2025;193:107515. doi: 10.1016/j.biombioe.2024.107515.
[58] Almena A, Siu R, Chong K, Thornley P, Röder M. Reducing the environmental impact of international aviation through sustainable aviation fuel with integrated carbon capture and storage. Energy Convers Manag 2024;303. https://doi.org/10.1016/j.enconman.2024.118186.
[59] Basu P. Biomass Gasification, Pyrolysis and Torrefaction: Practical Design and Theory. 3rd ed. London - UK: Elsevier Inc.; 2018. doi: doi: 10.1016/B978-0-12-812992-0.00001-7.
[60] Manouchehrinejad M, Mani S. Process simulation of an integrated biomass torrefaction and pelletization (iBTP) plant to produce solid biofuels. Energy Conversion and Management: X 2019;1:100008. https://doi.org/10.1016/j.ecmx.2019.100008.
[61] Valente A, Iribarren D, Dufour J. Harmonised life-cycle global warming impact of renewable hydrogen. J Clean Prod 2017;149:762–72. https://doi.org/10.1016/j.jclepro.2017.02.163.
[62] Christoforou EA, Fokaides PA. Life cycle assessment (LCA) of olive husk torrefaction. Renew Energy 2016;90:257–66. https://doi.org/10.1016/j.renene.2016.01.022.
[63] Tsalidis GA, Korevaar G. Environmental assessments of scales: The effect of ex-ante and ex-post data on life cycle assessment of wood torrefaction. Resour Conserv Recycl 2022;176:105906. https://doi.org/10.1016/j.resconrec.2021.105906.
[64] Ali Qamar O, Jamil F, Hussain M, Al-Muhtaseb AH, Inayat A, Waris A, et al. Feasibility-to-applications of value-added products from biomass: Current trends, challenges, and prospects. Chemical Engineering Journal 2023;454. https://doi.org/10.1016/j.cej.2022.140240.
[65] Chaudhuri P, Pande R, Baraiya NA. From char to flame: Evaluating bamboo biochar combustion via cone calorimetry and thermogravimetric analysis. Energy 2025;314. https://doi.org/10.1016/j.energy.2024.134313.
[66] Loebel Roson M, Schmidt SA, Choudhary V, Johnson TA, de la Mata AP, Harynuk JJ, et al. Comprehensive analysis of emissions from wood and cow dung burning using chemometrics and two-dimensional gas chromatography. Chemosphere 2024;366. https://doi.org/10.1016/j.chemosphere.2024.143445.
[67] Manatura K, Chalermsinsuwan B, Kaewtrakulchai N, Kwon EE, Chen WH. Machine learning and statistical analysis for biomass torrefaction: A review. Bioresour Technol 2023;369:128504. https://doi.org/10.1016/j.biortech.2022.128504.
[68] Alanya-Rosenbaum S, Bergman RD, Wiedenbeck J, Hubbard SS, Kelley SS. Life cycle assessment of utilizing freshly cut urban wood: A case study. Urban For Urban Green 2022;76. https://doi.org/10.1016/j.ufug.2022.127723.
[69] Chen WH, Biswas PP, Zhang C, Kwon EE, Chang JS. Achieving carbon credits through biomass torrefaction and hydrothermal carbonization: A review. Renew Sustain Energy Rev 2025;208. https://doi.org/10.1016/j.rser.2024.1150566.